AD NUMBER

AD901198

NEW LIMITATION CHANGE

TO

Approved for public release, distribution unlimited

FROM

Distribution authorized to U.S. Gov't. agencies only; Test and Evaluation; MAR 1971. Other requests shall be referred to Aviation and Surface Effects Department, Naval Ship Research and Development Center, Bethesda, MD 20034.

AUTHORITY

NSRDC ltr dtd 24 Apr 1974

DESIGN OF A CIRCULATION CONTROL STERN PLANE FOR SUBMARINE APPLICATIONS

by

Robert J. Englar
and
Robert M. Williams

Technical Note AL-200

March 1971

NAVAL SHIP RESEARCH AND DEVELOPMENT CENTER

BETHESDA
MARYLAND
20034

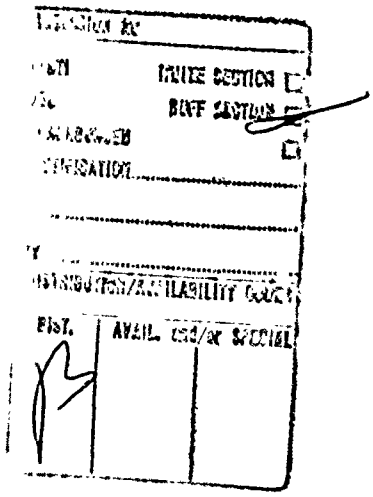
BUFF SECTION
DIST. AVAIL. and/or SPECIAL

DESIGN OF A CIRCULATION CONTROL STERN PLANE FOR SUBMARINE APPLICATIONS,

by

Robert J. Englar

and

Robert M. Williams

March 1971

79 P.

Technical Note AL-200

TN-

387 195

SUMMARY

The present study was undertaken to design a non-deflecting circulation control (CC) submarine stern plane to provide maneuverability control and eliminate the possibility of catastrophic crash dives due to stern plane jamming. Symmetric elliptic sections with tangential blowing out of upper and lower slots over a rounded trailing edge were used because of their high lift and equivalent aerodynamic (hydrodynamic) efficiencies. The CC model stern plane so designed was restricted by the requirement to maintain the same planform as a conventional stern plane, by the existence of a large boundary layer on the main body, and by the additional requirement of zero deflection. With moderate blowing, it was able to meet or exceed the prescribed lifting (maneuvering) requirements for the conventional deflecting control surface. In the event of a blowing failure, inherent stability would result due to the fixed nature of the plane. Presented in the study is a detailed design procedure, supporting experimental data, and the final geometry of the blown model stern plane. Also included is a similar study on an alternate blown configuration with end plates which showed a considerable performance improvement over the first design.

TABLE OF CONTENTS

LIST OF FIGURES

LIST OF FIGURES (Cont.)

LIST OF SYMBOLS

A	Stern plane planform area, ft^2
a	Lift curve slope, $\frac{dC_\ell}{d\alpha}$
A_j	Slot area, ft^2
AR	Stern plane aspect ratio
b	Stern plane semi-span, ft
b	Stern plane total span including body, ft (in end plate discussion only)
C, c	Stern plane local chord, ft
C_{d_e}	Two-dimensional equivalent drag coefficient
C_{D_e}	Stern plane equivalent drag coefficient
C_{D_i}	Stern plane induced drag coefficient
C_d	Sectional drag coefficient
C_{d_p}	Two-dimensional profile drag coefficient
C_ℓ	Two-dimensional section lift coefficient
C_L	Stern plane lift coefficient
C_p	Pressure coefficient, $\frac{P-P_\infty}{q_\infty}$
C_u	Momentum coefficient, $\frac{\dot{m}V_j}{q_\infty A}$
C_{μ_1}	Momentum coefficient for upper surface slot
C_{μ_2}	Momentum coefficient for lower surface slot

D_e	Equivalent drag, including penalty for blowing
D_{in}	Inlet momentum loss
D_p	Profile drag
e	Oswald efficiency factor
H	End plate total height, ft
HP_p	Pump or compressor horsepower
h_j	Slot height, ft
L	Total stern plane lift, lbs
ℓ	Section lift, lbs
P_d	Model duct (plenum) total pressure, psig
P_p	Pump pressure, psig
P_s	Static pressure, psig
P_∞	Free stream static pressure, psf
Q	Flow rate, ft^3/min
q_∞	Free stream dynamic pressure, lb/ft^2
r	Trailing edge radius, ft
S	Stern plane planform area, ft^2
t	Stern plane thickness, ft
V_i	Downwash velocity at the endplated stern plane, ft/sec
V_j	Jet exit velocity, ft/sec
V_ℓ	Local free stream velocity at the stern plane, ft/sec
V_R	Resultant velocity at the stern plane, ft/sec
V_∞	Free stream velocity, ft/sec

w	Downwash velocity, ft/sec
w_1	Downwash velocity far downstream, ft/sec
X	Distance from stern plane leading edge, ft
y	Spanwise distance from root chord, ft Spanwise distance from body centerline (end plate discussion only)
z	Nondimensional spanwise station, 2y/b
α	Section angle of attack, degrees
α_e, α_{eff}	Effective angle of attack, degrees
α_g	Geometric angle of attack, degrees
α_i	Induced angle of attack, degrees
Γ_o	Maximum circulation
η	Nondimensional spanwise station, y/b
λ	Scale factor, full scale/model
ρ	Free stream density, slugs/ft^3
χ	$\frac{1}{e}$

INTRODUCTION

The purpose of this study is to design a circulation control (C.C.) stern plane for a submarine. The design will subsequently be incorporated in a model test to determine the feasibility of replacing conventional mechanical surfaces.

Circulation Control offers the distinct possibility of a jam-free, inherently stable control surface with very high lift capability. These features would eliminate the potentially catastrophic jamming of present control surfaces while also significantly increasing the maneuver capability of the submarine. Other important improvements over conventional control surfaces are the ability to generate large forces for low speed control while also providing precise (vernier) control at high speeds. In addition, the rapid response time and low control forces associated with such a fluidic system are ideal for incorporation into an automatic stabilization system.

From a mission effectiveness standpoint the circulation control system is attractive because it could allow safe operation near maximum depth at higher speeds than conventional submarines, which are restricted by stability and control safety margins.

The primary disadvantages of such a device are fouling and power consumption. Presumedly, fouling due to particle blockage of the 0.2 inch full-scale slots can be handled by proper straining of the water and use of particle separators. The power consumption of the circulation control foil consists of three terms: profile, induced, and compressor (pump). In general, at the design value of lift, the profile drag will

be considerably less than that of a conventional shape, sometimes even negative (thrusting). The induced drag will be either equal to the conventional or somewhat less because of the more optimum lift distribution permitted by the slot geometry.

In summary, based on considerations of the above, a C.C. stern plane has been designed to demonstrate the feasibility of a blown control surface having no mechanical components but with inherent stability and increased maneuver margins. The following text describes in detail the design procedure and arrives at two slot height distributions for testing, one without end plates and one with them.

COMPARISON WITH CONVENTIONAL STERN PLANES

It is apparent that for the C.C. design to have competitive performance with conventional stern planes it must essentially balance the compressor power required with the reduction in profile power afforded by the jet blowing. This argument implies that the tradeoff essentially becomes two-dimensional in nature so that existing test data (References 1, 2, 3) can be employed to study the comparative power consumptions. To facilitate this comparison the profile and compressor power requirements are expressed in terms of an equivalent lift-drag ratio, where the equivalent drag is defined by:

$$D_e = D_p + \frac{HP_p}{V_\infty} + D_{in}$$

In dimensionless terms this becomes:

$$C_\ell / C_{d_e} = C_\ell \Big/ \left(C_{d_p} + C_\mu \frac{V_j}{2V_\infty} + C_\mu \frac{V_\infty}{V_j} \right).$$

Results of several two-dimensional wind tunnel tests are plotted in Figure 1. It may be seen that the C.C. airfoil is generally competitive in efficiency with conventional foils but at higher lift coefficient. Thus, the C.C. airfoil proposed for this design optimizes at a higher value of lift coefficient than the conventional NACA 0018 tail plane section.

In terms of the tail plane geometry the above results would suggest that for equal induced power and equal surface area (possibly stability requirements):

$$C_{D_i}\Big|_{con} = C_{D_i}\Big|_{cc} \tag{1}$$

$$\left.\frac{C_L^2}{\pi\ AR\ e}\right|_{con} = \left.\frac{C_L^2}{\pi\ AR\ e}\right|_{cc} \tag{2}$$

$$\frac{AR\ e\ |_{cc}}{AR\ e\ |_{con}} = \left(\frac{C_{L_{cc}}}{C_{L_{con}}} \right)^2 \tag{3}$$

For equal induced power and equal span (possibly a geometric constraint) at equal velocities:

$$C_{D_i} A \Big|_{con} = C_{D_i} A \Big|_{cc} \tag{4}$$

$$\frac{C_L^2 A^2}{\pi b^2 e}\Big|_{con} = \frac{C_L^2 A^2}{\pi b^2 e}\Big|_{cc} \tag{5}$$

$$\frac{A_{cc}}{A_{con}} = \frac{C_{L_{con}}}{C_{L_{cc}}} \sqrt{\frac{e_{cc}}{e_{con}}}$$

$$AR_{con} = \frac{b^2}{A_{con}}$$

$$AR_{cc} = \frac{b^2}{A_{cc}} = \frac{b^2}{\left(A_{con}\right)\left(\frac{C_{L_{con}}}{C_{L_{cc}}} \frac{e_{cc}}{e_{con}}\right)^{\frac{1}{2}}} = \frac{AR_{con}}{\left(\frac{C_{L_{con}}}{C_{L_{cc}}}\right)\left(\frac{e_{cc}}{e_{con}}\right)^{\frac{1}{2}}}$$

$$\frac{AR\ e\Big|_{cc}}{AR\ e\Big|_{con}} = \frac{C_{L_{cc}}}{C_{L_{con}}} \sqrt{\frac{e_{cc}}{e_{con}}} \tag{6}$$

Thus the optimum aspect ratio for the maximum effective lift-drag ratio varies in the manner of either Equation (3) or (6), depending on the initial assumptions. In these cases it would be expected that the over-all wing efficiency, denoted by

$$L/D_e = \frac{C_L}{C_{D_e} + C_{D_i}} = \frac{1}{\frac{C_{D_e}}{C_L} + \frac{C_{D_i}}{C_L}} \tag{7}$$

would probably optimize at a higher value of C_L.

The tail plane design described herein was not optimized in the above manner. Instead it was specified that the geometry be constrained to the conventional tail plane size and shape.

In the case that the design range of lift is identical with the conventional, the induced powers are equal. The C.C. airfoil sections are then required to operate considerably below the section lift coefficients for the optimum efficiencies.

An even more severe performance constraint added to the above was to specify no movable control surfaces. This affords the submarine inherent stability because in the event of a blowing failure (e.g., in a dive) the foil always generates a stabilizing moment (tending to neutralize the dive). In general, because it is fixed in line with the submarine body axis, the stern plane is required to generate positive lift at negative angles of attack. Indeed, when the induced flow and body boundary layer are included in the analysis the extreme design requirements at individual sections require lift coefficients on the order of 1.3 at section angles of attack of -30°. However, for the present study it was felt that if inherent stability were possible then the power penalty might be worthwhile. If the power requirements proved too great then either the stern plane angle would have to be adjusted or else the aspect ratio increased. The present study includes the use of end plates to increase the effective aspect ratio in lieu of a separate, more optimum high aspect ratio design.

DESIGN REQUIREMENTS

The stern plane design requirements were obtained from previous submarine test data (Reference 4). They are given in terms of the overall stern plane lift coefficient (positive downward) and body angle of attack (positive as shown in Figure 2). The fixed circulation control stern plane must be able to generate at only body angle of attack the same C_L generated by the conventional stern planes at body angle of attack plus stern plane deflection. Thus, the data of Figure 2 shows the test C_L obtained at given body angles of attack with stern plane deflection. With the fixed stern plane, operational lift requirement ranges are necessarily the same as the test data. However, it is felt that the maximum C_L requirement will occur at zero body angle of attack (e.g., cruise) at the initiation of a maneuver. As the body begins to pitch, lift is developed on it and the stern plane requirements are reduced. Thus, Figure 2 also depicts the fixed stern plane requirements based on maximum C_L from variable stern plane tests.

It is then necessary to calculate at each spanwise station the effective angle of attack $\alpha_e = \alpha_g + \alpha_i$ and the required section lift coefficient C_ℓ. This calculation is described in the section "Induced Flow Field Calculation and Boundary Layer Assumption". The requirements are nearly symmetrical for dive and rise so that a symmetric airfoil is required with blowing slots in upper and lower surfaces and the same planform as the conventional stern plane.

No other design requirements were imposed. It is assumed that the submarine operates with continuous but small blowing in cruise, giving approximately zero profile drag. This is probably desirable also

to prevent slot fouling. A possible stability problem arises in this condition which can be described as follows: If the foil attitude is perturbed, the surface pressure distribution on upper and lower surfaces will become asymmetric. With equal blowing rates it is probable that one jet will work somewhat more efficiently that the other, thereby creating a net lift This situation is shown in Figure 3, where it can be seen that the induced blowing lift is destabilizing while conventional $C_\ell = a\alpha$ is stabilizing.

Defining a lift response to a change in angle of attack when upper and lower blowing rates are equal by $\frac{\partial C_\ell}{\partial \alpha_e}\ (\alpha_e, C_{\mu_1} + C_{\mu_2})$ where C_ℓ is affected by both a pressure distribution change $\frac{dC_p(x/c)}{d\alpha_e}$ and a total momentum flux $C_{\mu_1} + C_{\mu_2}$, the condition for stability is

$$\frac{\partial C_\ell(\alpha)}{\partial \alpha}\ \alpha \geq \frac{\partial C_\ell \left(\frac{dC_p(x/c)}{d\alpha_e},\ C_{\mu_1} + C_{\mu^2} \right)}{\partial \alpha}\ \alpha_e \qquad (8)$$

No information is presently available for equal blowing jets. However, it would appear that except for very large blowing rates the conventional $a\alpha$ lift would always dominate in the present steady flow example. The small blowing rates required for zero profile drag in cruise should not be sufficient to produce the unstable condition.

INDUCED FLOW FIELD CALCULATION AND BOUNDARY LAYER ASSUMPTION

Three-dimensional airfoil design requires a detailed knowledge of the local flow field at each section of the foil. This will include primarily the spanwise distributions of sectional lift coefficient and effective angle of attack. Finite wing theory predicts a uniform induced downwash and thus minimum induced drag when the circulation distribution is elliptic. [This usually requires an elliptic distribution of chord (c) for constant airfoil section and local angle of attack (α), or an elliptic distribution of the combination $a\alpha c$ where (a) is the lift curve slope.] However, a circulation control foil is not limited to the elliptic chord constraint, since essentially any desired circulation can be obtained for a given foil merely by adjustment of the local mass flow rates (by variation in pressure ratio or slot height distribution). It was thus decided to design the stern plane to maintain the elliptic circulation distribution and minimize induced drag.

An additional constraint on the tail plane design is that the local free-stream velocity is not constant as for a conventional aircraft wing. The stern plane is located far downstream of the maximum submarine body diameter and thus a very thick boundary layer has developed on the body at the tail plane juncture. Past tests have shown that this boundary layer extends approximately to 50 percent of the stern plane span. It was assumed that the local velocity distribution in the boundary layer had a parabolic form, and was thus represented as (see Figure 4):

$$V_\ell = V_\infty \sqrt{2\eta} \quad \text{for } \eta = y/b < 0.5$$

$$V_\ell = V_\infty \quad \text{for } \eta \geq 0.5 \tag{9}$$

Using this representation, the resultant velocity (V_R) of the local and downwash velocities is

$$V_R(\eta) = \sqrt{V_\ell^2(\eta) + w^2} \tag{10}$$

and the resultant induced angle is:

$$\alpha_i(\eta) = \tan^{-1} \frac{w}{V_\ell(\eta)} \tag{11}$$

which assumes no trailing vortex sheet deflection.

From Figure 4

$$\Gamma(\eta) = \Gamma_o \left[1 - (2\eta - 1)^2\right]^{\frac{1}{2}}$$

Then for a given total stern plane lift coefficient, but unknown Γ_o,

$$C_L = \frac{L_1}{qS_1} = \frac{b}{qS_1} \int_{\eta=0}^{1} \rho V_R(\eta)\, \Gamma(\eta)\, d\eta$$

$$= \frac{2b}{V_\infty^2 S_1} \int_{\eta=0}^{1} \left[V_\ell^2(\eta) + w^2\right]^{\frac{1}{2}} \Gamma_o \left[1-(2\eta-1)^2\right]^{\frac{1}{2}} d\eta \tag{12}$$

Where L_1 and S_1 are lift and planform area of one plane.

Then,

$$C_L = \frac{2\Gamma_o b}{V_\infty^2 S_1} \left\{ \int_{\eta=0}^{\frac{1}{2}} \left[2\eta V_\infty^2 + \frac{\Gamma_o^2}{4b^2} \right]^{\frac{1}{2}} \left[1-(2\eta-1)^2 \right]^{\frac{1}{2}} d\eta \right.$$

$$\left. + \int_{\eta=\frac{1}{2}}^{1} \left[V_\infty^2 + \frac{\Gamma_o^2}{4b^2} \right]^{\frac{1}{2}} \left[1-(2\eta-1)^2 \right]^{\frac{1}{2}} d\eta \right\} \quad (13)$$

The usual assumption made in finite wing theory is that $V_\ell >> w$ so that $V_R \simeq V_\ell$ and $\frac{\Gamma_o^2}{4b^2}$ is neglected, thus making evaluation of the above integrals simple for elliptic distribution. For the low aspect ratio stern plane with $V_\ell \to o$ inboard, that assumption and the corresponding small angle assumption ($\alpha_i \simeq \frac{w}{V_\ell}$) cannot be made, as the downwash velocity will be greater than V_ℓ inboard, and associated induced angles will approach 90 degrees. The solution thus had to be an evaluation of the full integral equation. An iterative scheme was developed where an initial value of Γ_o was input, the integral equation evaluated by a Simpson's rule numerical integration, and the resulting C_L compared to the desired value. Adjustment was then made on Γ_o and the procedure was recycled until the desired C_L was obtained. Using the correct value of Γ_o, the corresponding spanwise distributions were calculated:

$$w = \frac{\Gamma_o}{2b} = \text{constant} \tag{14}$$

$$V_R(\eta) = \sqrt{V_\ell^2(\eta) + w^2} \tag{10}$$

$$\alpha_i = \tan^{-1} \frac{w}{V_\ell(\eta)} \tag{11}$$

$$\alpha_{eff} = \alpha_g - \alpha_i \tag{15}$$

$$\Gamma(\eta) = \Gamma_o \left[1-(2\eta-1)^2 \right]^{\frac{1}{2}} \tag{16}$$

$$C(\eta) = C_r - \eta(C_r - C_t) \tag{17}$$

$$C_\ell(\eta) = \frac{\rho V_R(\eta)\Gamma(\eta)}{q(\eta)C(\eta)} = \frac{2\Gamma(\eta)}{V_R(\eta)C(\eta)} \tag{18}$$

These distributions of C_ℓ and α_{eff} must then be obtained by the individual sections of the proposed stern plane design. Sample distributions presented in Figure 5 show that rather severe requirements will be imposed on the inboard sections if the elliptic Γ distribution is to be maintained. Small local velocities and very high induced angles result in large negative effective angles of attack and relatively high C_ℓ requirements.

SECTION CHARACTERISTICS

From the C_ℓ and α_{eff} distributions of Figure 5, it is apparent that for almost all operating conditions of the fixed stern plane, positive lift coefficients are required at negative α_{eff} (or the equivalent

for the symmetric foil: negative lift at positive α_{eff}). This would eliminate from consideration the conventional symmetric foil, which cannot generate positive C_ℓ at negative angle of attack. It is shown (References 1, 2, 3) that circulation control sections operate efficiently at negative angles of attack while generating extremely high positive lift. This is more true of thicker elliptic sections which because of their larger nose radii and increased blowing effectiveness are able to eliminate or delay lift loss due to lower surface flow separation and stall. As the most severe requirements on the stern plane are inboard, it is desirable to use as thick an ellipse there as allowable and then taper to a somewhat thinner section outboard where conditions are less severe. From the preceding consideration and from model construction constraints it was decided to limit the root thickness-to-chord ratio to 0.25 and taper linearly to a 0.20 tip section. Elliptical sections were also chosen although an ovoid shape would appear more optimum inboard in order to delay leading edge separation. Figure 6 depicts the prescribed model stern plane planform and dimensions. The root section plane was defined as the intersection of the lifting line (mid-chord line in this case) with the body.

With the section thicknesses thus specified, corresponding lift, drag and efficiency data are needed. A reliable theoretical calculation method for the performance of circulation control sections does not presently exist due primarily to difficulty in calculation of tangential wall jet effects. However, an extensive series of two-dimensional tests have been run at NSRDC on ellipses ranging from 15 to 50 percent thick, with variations in camber, slot height, slot location, trailing edge

radius, angle of attack, Reynolds number and momentum coefficient. Most closely related to the stern plane sections are a 30 percent thick ellipse with 1.5 percent camber and a 20 percent uncambered ellipse with trailing edge radius-to-chord ratio of 0.04, instead of the pure elliptic value of 0.02. Lift data was obtained either by surface pressure taps or floor and ceiling taps, while drag was obtained from momentum loss in the wake as measured by a total head rake. Figures 7 to 12 present the test data for these two models corrected for the induced effects of non-two-dimensional flow which is characteristic of high lift airfoil tests. (Additional detail can be obtained from References 1 and 2.) Figures 13 and 14 present experimental chordwise pressure distributions for the 30 percent ellipse at $\alpha = -20°$ and $-30°$ and comparable values of C_μ. Flow separation at $\alpha = -20°$ and $C_\mu = 0$ immediately returns to attached flow with light blowing, while C_ℓ is generated by the high trailing edge favorable pressure gradients. However, at $\alpha = -30°$, lower surface reattachment is not produced, but positive C_ℓ is still generated with blowing due to even greater trailing edge suction peaks.

In order to obtain necessary lift data to determine required blowing rates for the stern plane sections, Figures 7 and 10 were overlaid. For a given stern plane C_L requirement, the section C_ℓ and α_{eff} for each spanwise station were obtained from figures similar to 5, the thickness ratio was calculated from the linear variation, and then the combination of these three parameters was interpolated from the 20 and 30 percent ellipse experimental data overlay to yield the corresponding momentum coefficient, C_μ. It should be noted that this interpolation may introduce some error, in that the data for the desired pure elliptic

symmetric sections was obtained from the slightly cambered 30 percent section and the 20 percent section with a slightly rounded trailing edge. It is felt, however, that these sections are sufficiently characteristic of the desired sections that the overall error will not be large. In addition, data for $\alpha = -20°$ and $-30°$ for the 20 percent ellipse was extrapolated based on the values of $\frac{\Delta C_\ell}{\Delta \alpha}$ at constant C_μ from the existing data, and on comparison with test data for the 30 percent section at $\alpha = -30°$.

Mention should be made of the effect of chordwise slot location on the sectional properties of elliptic CC airfoils. Reference 5 indicates that for constant momentum coefficient and angle of attack, forward movement of the slot will delay stall due to prevention of boundary layer separation, but lift is reduced since the jet sheet has a greater momentum deficit when it reaches the trailing edge. On the other hand, rearward slot movement will produce a considerable increase in lift augmentation and $C_{\ell_{max}}$ but will not be as effective in preventing upstream boundary layer separation on the upper surface. In the present design high positive angles of attack are not expected thus indicating that a more rearward slot location is desired. Further criteria as to the choice of this location is presented in the section DESIGN PROCEDURE.

MODEL GEOMETRY AND SCALING

The model stern plane geometry is shown in Figure 6. Denoting a scale ratio of $\lambda = \ell_{FS}/\ell_M$ (where FS subscript denots full-scale and M subscript denotes model), the relations for the compressor power and flow

rate are given below:

Compressor

$$HP_p = \frac{\Delta P\, Q}{550 \cdot 60} = \frac{\rho A_j V_j^3}{1100} \tag{19}$$

where

$$\Delta P = (P_p - P_s) = \frac{\rho}{2} V_j^2$$

and

$$Q = 60 A_j V_j$$

For Froude scaling

$$\frac{V_M}{V_{FS}} = \lambda^{-0.5} \tag{20}$$

and for $C_{\mu_M} = C_{\mu_{FS}}$ (equal lift distribution)

$$\frac{V_{j_M}}{V_{j_{FS}}} = \lambda^{-0.5} \tag{21}$$

$$\frac{HP_M}{HP_{FS}} = \frac{\left(A_j V_j^3\right)_M}{\left(A_j V_j^3\right)_{FS}} = \lambda^{-3.5} \tag{22}$$

also

$$\frac{Q_M}{Q_{FS}} = \frac{\left(A_j V_j\right)_M}{\left(A_j V_j\right)_{FS}} = \lambda^{-2.5} \tag{23}$$

For the present full-scale vehicle ($\lambda = 16.67$) operating at 25 knots the model design speed is $V_M = (25)1.689\ \lambda^{-0.5} = 10.2$ ft/sec.

DESIGN PROCEDURE

The model design was determined from the prescribed operating requirements (Figure 2), and the scaled operating speed of 10.2 ft/sec. The procedure used in the design of the tail plane is described below together with the actual calculated results:

LIFT AND ANGLE OF ATTACK DISTRIBUTIONS

Using operating requirements (Figure 2) calculate the induced flow field (for minimum induced drag), angle of attack, and section lift coefficient distribution for several typical design points, Figure 5.

THICKNESS DISTRIBUTION

Using experimental section characteristics, determine the approximate spanwise thickness distribution required. In the present case, thicker sections were required inboard to handle large negative angles of attack, but model construction requirements limited maximum t/c at the root to 25 percent (Figure 15). If a higher aspect ratio (and thus lower α_i) were allowed, the required thickness ratios would diminish.

MOMENTJM COEFFICIENT DISTRIBUTION

After selecting an appropriate thickness distribution, several potential "limit design" cases (medium C_L at negative α_g, high C_L at zero α_g) are selected. Experimental section characteristics are then employed to interpolate for the required value of C_μ for the given local lift coefficient and angle of attack (Figure 16).

DIMENSIONLESS SLOT HEIGHT-TO-CHORD RATIO

Using the relationship for momentum coefficient per unit span

$$C_\mu(\eta) = \frac{\rho A_j V_j^2}{\frac{1}{2}\rho V_R^2(\eta)\, C(\eta)} = \frac{2h_j(1)V_j^2}{V_R^2 C} = 2\frac{h_j}{C}\left(\frac{V_j}{V_R}\right)^2 \qquad (24)$$

i.e., C_μ can be obtained from variation of slot height or jet velocity.

Rearranging,

$$\frac{h_j}{C} = \frac{C_\mu(\eta)}{2\left[V_j/V_R(\eta)\right]^2} \qquad (25)$$

From the resulting C_μ - η distribtuions of Figure 16, a tentative design condition (C_L and α_g) is selected. Then, for V_∞ = 10.2 ft/sec and various constant values of V_j/V_∞, V_j is found. For the tentative design condition, the velocities w and $V_R(\eta)$ and the resulting ratios $V_j/V_R(\eta)$ are calculated. These ratios and C_μ (η) from Figure 16 are then used in Equation (25) to generate curves of h_j/c vs η for constant values of V_j/V_∞, Figure 17. (Constant V_j/V_∞ implies constant plenum total pressure.)

CHOICE OF DESIGN SLOT HEIGHT-TO-CHORD DISTRIBUTION

To determine which h_j/c distribution of Figure 17 is more optimum from the standpoint of lift augmentation ratio $\left(\frac{\Delta C_\ell}{\Delta C_\mu}\right)$, a working plot of h_j/r versus h_j/c is generated (Figure 18). For a nominal range of $h_j/r \leq .05$(which yields strongly attached Coanda flow) and for a geometric range of $.02 \leq r/c \leq .05$, (which yields good flow turning without high suction peaks and high drag) an appropriate maximum h_j/c is selected. Normally this is in the range of $.0005 \leq h_j/c \leq .0025$. From these results a tentative design of the dimensionless slot height/chord distribution

can be selected. For a detailed discussion of the above parametric range, see Reference 6.

OFF-DESIGN PERFORMANCE

Operation at other combinations of C_L and α_g with the same slot height distribution is difficult to analyze. In general the lift distribution will be other than elliptic so that the inflow analyses employed herein would require modification. The off-design performance may actually determine the maximum installed power requirement. For the present configuration this problem has not been fully studied; however, it is apparent from Figure 16 that the calculated power for the design condition ($\alpha_g = 0°$, $C_L = 0.95$) will also suffice for the condition of $\alpha_g = -6°$, $C_L = 0.72$. For $\alpha_g = -12°$, $C_L = 0.95$ the design power would not appear to be adequate. However, the latter is an extreme condition obtained from static tests and in all probability will not be required for the dynamic operating envelope of the CC stern planes (Figure 2).

DIMENSIONAL SLOT HEIGHT

Up to this point the geometric ratios have been dimensionless. The actual model scale is next introduced using $V_\infty = 10.2$ ft/sec and $b = 9.86$ inches, the trailing edge semi-span. A dimensionless slot height curve is next generated to determine if a viable slot height distribution is possible (Figure 19).

PUMP FLOW RATE AND POWER REQUIREMENTS

The slot height is then integrated over the span to give slot area. A working curve of V_j versus P_d is generated (Figure 20), where P_d is duct (plenum) total gage pressure and P_s is static pressure at operating depth (11 feet for present model). It is then a simple matter

to generate curves of duct pressure versus total flow rate (Figure 21) and horsepower (Figure 22),

where

$$Q = 60\ A_j V_j,\ ft^3/min$$

$$HP_p = \frac{\Delta P\ Q}{33000}$$

and

$$\Delta P = P_d - P_s$$

These curves are for constant values of A_j, which is now the slot area of both stern planes together. The constant A_j values are the slot areas required to meet the design condition at velocity ratios of 4, 6, and 8.

From these results the pump requirements can be determined. Conversely for a given pump size the available working range can be determined. For the present model the latter approach was used with the pump characteristics of Figure 23, and it was concluded that two pumps (Crane Deming Model 7-AHF4, 2HP, 20-gallons) in parallel were required to generate the necessary flow rates. Then, $V_j/V_\infty = 8$ was chosen for the design condition based upon the total Q limitation with both pumps of about 7 $ft.^3/min.$ and the slot height limitations of Figure 18.

DETAILED TRAILING EDGE DESIGN

The slot position and detailed trailing edge geometry can next be calculated. For this purpose the potential flow pressure distributions are calculated for each spanwise section and the slot is located based on the pressure distributions. Various trailing edge radii can be used to affect the position of adverse pressure gradient (Figure 24).

For the present study elliptical airfoil sections were employed to simplify the small scale design. However, it is possible, based on the pressure distributions, that an ovoid section would be more effective on the inboard profile in preventing separation.

The final trailing edge design is contingent on four constraints (Reference 6): (1) the slot height is prescribed; (2) the trailing edge radius should differ only slightly from pure elliptical (for low drag) and should have a value of $.02 \leq r/c \leq .05$; (3) the slot chordwise position should be located slightly ahead of the adverse gradient for the worst combination of C_ℓ and α_g; (4) the slot efflux should exit as close to tangency with the airfoil shape as possible and still have the nozzle entrance smoothly convergent. In general it is difficult to satisfy all of these constraints and some compromise is required. The final designs for the section profiles (constrained to linear variations between root and tip) and overall stern plane layout are shown in Figures 25 and 26.

The foregoing analysis was based on the initial assumption of a large parabolic boundary layer profile on the body influencing the stern plane velocity profile, and an elliptic circulation distribution approaching $\Gamma(\eta) = 0$ at both the tip and root of <u>each</u> plane. Experiment and flow visualization tend to confirm these assumptions. However, it is of interest to note the effects of the simplified conditions of constant velocity [$V_\ell(\eta)$ = constant] and/or an elliptic $\Gamma(\eta)$ distribution approaching zero at the tip and the maximum at the root (thus spanning the total stern plane from tip to tip). These cases are investigated in Appendix A, with the resulting reductions in both mass flow and power requirements shown in Figures 21 and 22.

END PLATE DESIGN

GENERAL CONSIDERATIONS

A means of reducing both the pump power and induced drag on the present model (i.e., with wing span and planform area constrained) is to use end plates. These plates reduce the induced angles of attack along the span and therefore allow the sections to operate with less blowing. Also, the lower surface boundary layer separation (Figure 14) can be reduced, thereby reducing drag. However, the end plates themselves create additional profile and induced drag so that the design tradeoff reduces essentially to a reduction in pumping power for an increase in propulsive power. Mangler (Reference 7) has given the basic lifting line theory for the end plate. Other investigators (Reference 8 to 10) have conducted experiments which at least partially supported Mangler's theory.

It would be a relatively straightforward matter to optimize the end plate height and camber such that the reduction in compressor power could be traded off with the increase in tail plane drag, i.e., Figure 27. No attempt has been made at such an optimization in the present study due to time limitations.

For the calculation of induced flow angles and spanwise lift distributions by Mangler's theory it is necessary to make the following assumptions:

- The body itself generates three-dimensional lift in a similar manner to an aircraft fuselage.
- The body boundary layer is sufficiently entrained by the blowing slot so that finite lift is generated at the body-wing junction.

The effect of the above assumptions is to stipulate a continuous lift distribution over the entire wing span. Whether or not such a distribution is feasible is uncertain. The use of larger blowing slots at the wall junction would generate finite lift at that location in a manner similar to a blown wind tunnel model (Reference 1). Also the use of upstream pump intakes on the body would tend to remove the boundary layer and help generate attached flow. The practical goal in any case is to generate a continuous finite lift distribution so that no local wing-body separations occur which would create strong vortices tending to reduce the effective aspect ratio by a significant factor. Careful joining of the wing-body with a small radius fillet would also be worthwhile.

The induced flow calculation is derived using Mangler's results (Reference 7, Figures 10 and 11). The definition of parameters is seen in Figure 28.

The following definitions are useful:

$$z = \frac{2y}{b}$$

$$K = K_o/K_\mu$$

$$X = \frac{1}{e} = C_{D_i} \Big/ \frac{C_L^2}{\pi AR}$$ Which for end plates is always greater than 1.0

w_1 = downwash velocity far downstream (twice V_i)

V_i = downwash velocity at stern plane

y = spanwise distance from body centerline

b = total span, tip to tip, including body

END PLATE DESIGN PROCEDURE

The technique used to design the end-plated configuration is as follows:

(1) For the present model we take $K_o = K_\mu$; $K = 1$ from the symmetrical ascent-descent condtions and $h/b = H/2b = 0.2$, as a reasonable geometric constraint.

(2) To determine the lift and angle of attack distribution from Mangler we note that:

$$\chi = \pi / \int_{-1}^{1} \left[\frac{\Gamma(z)}{w_1 \; b/2} \right] dz$$

and

$$C_{D_i} = \frac{\chi C_L^{\,2} S}{\pi \, b^2} \tag{26}$$

Also

$$C_{D_i} = \frac{2b}{\rho V_\infty^{\,2} S} \int_0^1 (\ell \sin \alpha_i) \, dz \tag{27}$$

$$= \frac{w_1^{\,2} b^2}{2 V_\infty^{\,2} S} \int_{-1}^{1} \left[\frac{\Gamma(z)}{w_1 \; b/2} \right] dz$$

Equating these expressions for C_{D_i} yields

$$\frac{V_i}{V_\infty} = \frac{w_1}{2V_\infty} = \frac{C_L \, \chi}{AR\pi} \tag{28}$$

where

$$C_L = \frac{w_1 \; b^2}{2 V_\infty S} \int_{-1}^{1} \left[\frac{\Gamma(z)}{w_1 \; b/2} \right] \frac{V_\ell(z)}{V_\infty} \, dz \tag{29}$$

(3) The induced angle of attack is now given by

$$\alpha_i(z) = \tan^{-1} \frac{V_i}{V_\ell(z)} = \tan^{-1} \left(\frac{C_L V_\infty}{AR\ V_\ell(z)} \right) \Bigg/ \int_{-1}^{1} \left(\frac{\Gamma(z)}{w_1 b/2} \right) \left(\frac{V_\ell(z)}{V_\infty} \right) dz \quad (30)$$

and section lift coefficient by:

$$C_\ell(z) = \frac{\Gamma(z)}{w_1\ b/2}\ \frac{w_1\ b}{V(z)C(z)}$$

$$C_\ell(z) = \frac{\Gamma(z)}{w_1\ b/2}\ \frac{2\ V_\infty\ C_L\ \chi\ b}{AR\ \pi\ V(z)C(z)} \quad (31)$$

(4) It is now a straightforward matter to calculate the section lift coefficient and angle of attack distributions. First, for the case derived independently in the section INDUCED FLOW FIELD CALCULATION for an elliptic circulation distribution on each half plane we note

$$\chi = 1.0$$

$$AR = b^2/A = (.822)^2/.745 = .906$$

and for

$$C_L = 0.95$$

$$\alpha_{i_{tip}} = \tan^{-1} \frac{V_i}{V_\infty} = \tan^{-1} \frac{C_L\ \chi}{AR\ \pi}$$

$\alpha_{i_{tip}} = 18.45^\circ$ which agrees very closely with the results shown in Figure 5.

For the end plate calculation, in keeping with the assumptions the span and area are taken as the total span and an area described by both planes plus the included body planform area, then

$$AR = b^2/A = (28.586)^2/328 = 2.47$$

$$\chi = 0.73, \text{ for } h/b = H/2b = 0.2$$

and for the same value of $C_L = 0.95$, the induced tip angle of attack is

$$\alpha_{i_{tip}} = \tan^{-1} \frac{V_i}{V_\infty} = \tan^{-1} 0.0942 C_L = 5.12^\circ$$

It can be seen that the inclusion of end plates together with a finite loading on the body permit an induced angle reduction over the previous case, by a factor of almost four.

The computed spanwise distributions of lift coefficient and angle of attack corresponding to the design case ($\alpha_g = 0^\circ$, $C_L = 0.95$) are shown in Figure 29. It is assumed that at the body ($z \leq 0.18$) both the velocity and the lift are small and vary such that the ratio $\Gamma(z) = \frac{\ell(z)}{\rho\, V(z)}$ is in accordance with Mangler's theory. This assumption rests on somewhat tenuous grounds, but it seems reasonable to assume the velocity to be small due to the extremely thick boundary layer. The lift should also be small but finite due to a reduction in pressure on the body caused by a three-dimensional outflow to the low pressure region of the wing. Such a condition frequently occurs in aircraft at the wing-body junction.

The dimensional slot height distribution is shown in Figure 30 for the selected $V_j/V_\infty = 4$ design condition. Comparison with Figure 19 indicates about a 74 percent reduction in slot area for the corresponding

design C_L and duct pressure (V_j/V_∞), due primarily to reduced C_μ requirements. The slot "modification", shown in Figure 30, is discussed subsequently.

The flow rate and power requirements for the design slot height distribution ($V_j/V_\infty = 4$) are plotted as the dashed lines in Figure 31. It can be seen that approximately 48 percent reduction in flow rate and 87 percent reduction in power are theoretically possible relative to the original case with $V_j/V_\infty = 8$.

Mangler's theory does not describe end plate design other than to indicate that the height should be $H/b = 2h/b = K_o + K_\mu$. For the present model $K = K_o/K_\mu = 1.0$, $K_o = K_\mu = 0.2$ so that the end plate are symmetrically arranged about the chordal plane, 0.2b above and below. References 8, 9, and 10 provide some information on end plate design, with Reference 10 indicating that end plates perform well when they are at least 4/3 of the airfoil chord in length. The end plate planform was designed using this criteria, the calculated pressure distributions, and empirical results on curved wall jets operating near planar surfaces. The geometry is shown in Figure 32. For the present study the end plates are taken as thin plates although there is some evidence that a small amount of camber would further reduce the spanwise induced velocity (and hence pump power) albeit at the expense of higher induced and profile drag.

In summary, end plates appear to be an extremely powerful means of reducing the pumping power when aspect ratio is geometrically limited. The present analysis is possibly rather optimistic because of inability of the body to produce the theoretical lift required, and a possible vortex formation at the body-wing junction and end plate-wing junctions.

The latter phenomena may be prevented to some degree by increasing the slot height adjacent to these surfaces (Reference 1). The recommended modification for this purpose is noted in Figure 30. The use of pump intakes ahead of the stern plane would also be of help in removing low velocity boundary layer air which is susceptible to separation.

CONCLUSIONS AND RECOMMENDATIONS

- Circulation Control can provide a simple and highly reliable solution to the problem of submarine stability and control and may also be employed on other control surfaces.

- The present model should adequately demonstrate feasibility of the concept, even though non-optimum. Proposed tests should verify the analysis, and indicate any need for modification.

- A system design should be conducted considering the power available for pumping throughout the submarine depth-velocity envelope. Detailed ducting losses and transmission pump efficiency should be studied. Total vehicle drag should be computed.

- The present design is non-optimum and could be improved by the following design changes:

(1) Reduction in stern plane chord and the use of end plates with a small amount of camber. This would permit increased aspect ratio, airfoil section operation closer to $(\ell/d_e)_{max}$, and further reduction in compressor power required.

(2) Optimization of airfoil thickness distribution with the above changes. This would provide generally thinner sections with lower drag.

(3) Optimization of airfoil shape which would probably yield ovoid type sections inboard and elliptical outboard.

(4) Optimization of slot chordwise position to maximize blowing efficiency and minimize compressor power.

(5) Installation of a separate high mass flow blowing chamber on the inboard section of the stern plane to energize the low velocity boundary layer, and use of pump intakes ahead of stern plane.

Aviation and Surface Effects Department

Naval Ship Research and Development Center

Washington, D.C. 20034

March 1971

APPENDIX A

Variation in Spanwise Distributions of Circulation and Local Velocity For the Non-Endplated Model

The design analysis performed in the text for the non-endplated stern plane was based on the assumptions of main body boundary layer influence on a substantial part of the freestream flow over the stern plane, and an elliptic circulation distribution on each stern plane (see Figure 4). It is of interest to replace these assumptions with the simplifications frequently employed in finite wing analysis, i.e., constant free stream velocity over the entire span, and an elliptic circulation distribution from tip to tip with the maximum at the wing centerspan. The design analysis was repeated for these two simplifications (maintaining the original planform and section thickness distribution), with $C_L = .95$, $\alpha_g = 0$, and $V_j/V_\infty = 8$.

CASE I - The local freestream velocity was assumed constant ($V_\ell(\eta) = V_\infty = 10.2$ ft/sec) but the circulation distribution was maintained as in the initial case (Figure 4). The effect was that all velocities and the induced angle became constant across the span (see Figure 33). The inboard sections were thus not subjected to the adverse effects of the velocity decay at the body. The resulting distribution of C_ℓ, C_μ, and slot height are shown in Figure 34, where the major difference from the original case is the large reduction in C_μ and τ_ℓ at the inboard sections (compared with Figures 16 and 5). The 20% reductions from the initial case in both flow rate and power required (Figures 21 and 22)

were due to slot area reduction (at a constant $V_j/V_\infty = 8$). In general, the slot height distributions for the two cases were similar in shape, but Case I had the smaller area.

CASE II - The assumption of an elliptic circulation distribution with Γ_o (i.e., Γ_{max}) located at the wing center-span was made, along with the constant freestream approximation from Case I. The submarine body was assumed to carry no load nor was its diameter included in the resulting total span (2b). Constant values of w, V_R, and α_i were again yielded by the constant free-stream velocity assumption, as shown in Figure 35. The inclusion of the entire stern plane span within the elliptic Γ distribution effectively doubled the finite wing's aspect ratio, and the reduced downwash greatly decreased the induced angle relative to both Case I and the original case. As a result, each spanwise section operated at a less negative effective angle and was able to provide the required $C_\ell(\eta)$ at a much lower C_μ (Figure 36). The associated slot area was also reduced accordingly which, for constant $V_j/V_\infty = 8$, required flow rates and pump horsepower of 57% less than the original case (see Figures 21 and 22). The advantage of using both the simplified assumptions (for V_ℓ and Γ) is obvious, though the situation still remains that the original case probably is more characteristic of reality.

CASE III - The same assumptions as Case II were used, but the velocity ratio was reduced to $V_j/V_\infty = 4$. Unlike the original case, this lower jet velocity in the simplified case generated flow rates less than the pump limiting quantity (7 ft^3/min.) and geometric properties within the desirable range of Figure 18. This case was run for comparison (in Figure 31) with the endplated model, which has a similar Γ distribution

(with the exception of a finite value at the endplates, instead of zero at the tip). Figure 31 shows the effectiveness of the endplates, which produced for a model experiencing the detrimental body boundary layer a lower flow rate and power requirement than the much simplified case III.

REFERENCES

1. Williams, Robert M. Some Research on Rotor Circulation Control. In CAL/AVLABS Symposium: Aerodynamics of Rotary Wing and V/STOL Aircraft. 3rd, Buffalo, Jun 1969. Proceedings, Vol. 2.

2. Englar, Robert J. Two-Dimensional Subsonic Wind Tunnel Tests on a Cambered 30 Percent Thick Circulation Control Airfoil. (Naval Ship Research and Development Center. Tech. Note AL-201)(In preparation)

3. Williams, Robert M. and Kenneth R. Reader. Two-Dimensional Subsonic Wind Tunnel Tests on a 50 Percent Thick Circulation Control Airfoil With Blowing Slots Located at 88.6 and 98.5 Percent Chord. (Naval Ship Research and Development Center. Tech. Note AL-186)(In preparation)

4. Dempsey, Elizabeth M. Stability and Control Characteristics of the Selected Preliminary Design for SSN 688 (with Cruciform Stern) from Captive Model Tests (U). Wash., Mar 1970. (Naval Ship Research and Development Center. Test Rpt. C-386-H-02) CONFIDENTIAL

5. Jones, Dale G. The Performance of Circulation Control Airfoils. Cambridge, Jul 1970. (Cambridge Univ. Ph.D. Thesis)

6. Williams, Robert M. Design Considerations of Circulation Control Airfoils. (Naval Ship Research and Development Center. Tech. Note AL-185) (In preparation)

7. Mangler, W. The Lift Distribution of Wings with End Plates. Wash., April 1938. 19 p. incl. illus. (National Advisory Committee on Aeronautics. Technical Memorandum No. 856)

8. Lowry, J.G. and Raymond D. Vogler. Wind-Tunnel Investigation at Low Speeds to Determine the Effect of Aspect Ratio and End Plates on a Rectangular Wing With Jet Flaps Deflected 85°. Wash., Dec 1956. 21 p. incl. illus. (National Advisory Committee for Aeronautics. Tech. Note 3863)

9. Bates, William R. Collection and Analysis of Wind-Tunnel Data on the Characteristics of Isolated Tail Surfaces With and Without End Plates. Wash., May 1947. 21 p. (National Advisory Committee for Aeronautics, Tech. Note No. 1291)

10. Halliday, A.S. and D.K. Cox. Note on the Effect of Size and Position of End Plates on the Lift of a Rectangular Wing in a Wind Tunnel. London, H.M.S.O., 1956. [16] p. incl. illus. (Gt. Brit. Aeronautical Research Council. C.P. 305. 17,755, Jul 1955)

11. Williams, Robert M. and Harvey J. Howe. Two Dimensional Subsonic Wind Tunnel Tests on a 20 Percent Thick, 5 Percent Cambered Circulation Control Airfoil. Wash., Aug 1970. 23ℓ. incl. illus. (Naval Ship Research and Development Center. Tech. Note AL-176) (AD 877 764)

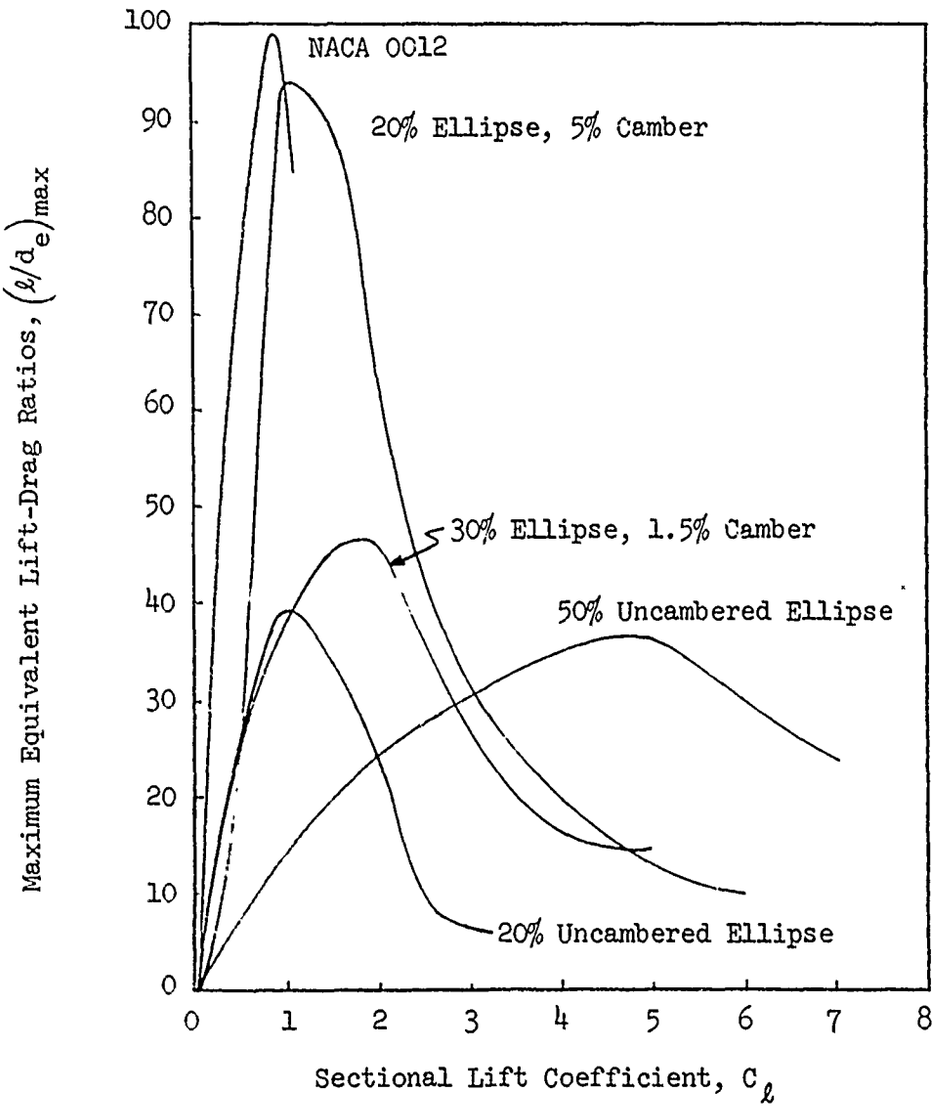

Figure 1 - Comparative Efficiencies for Conventional and Blown Airfoil Sections

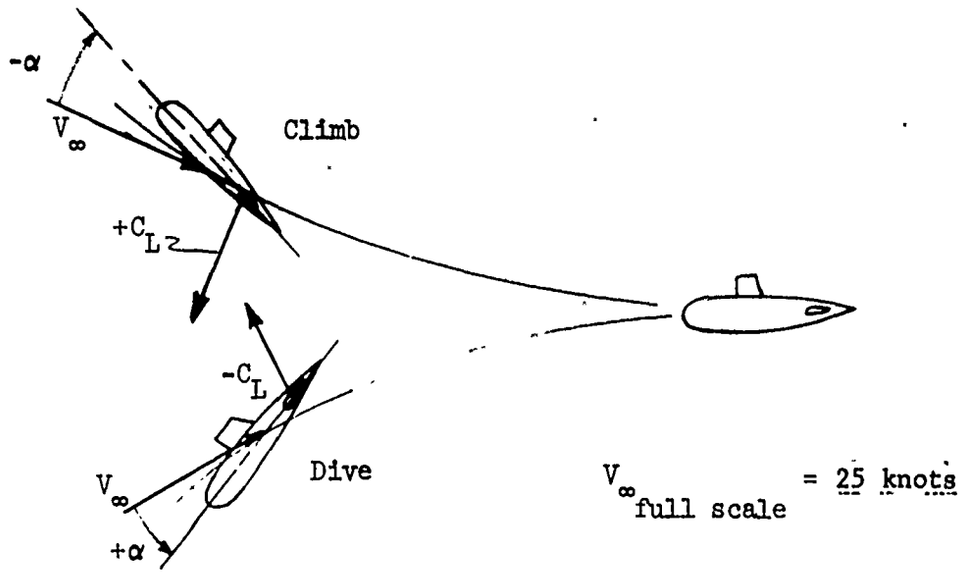

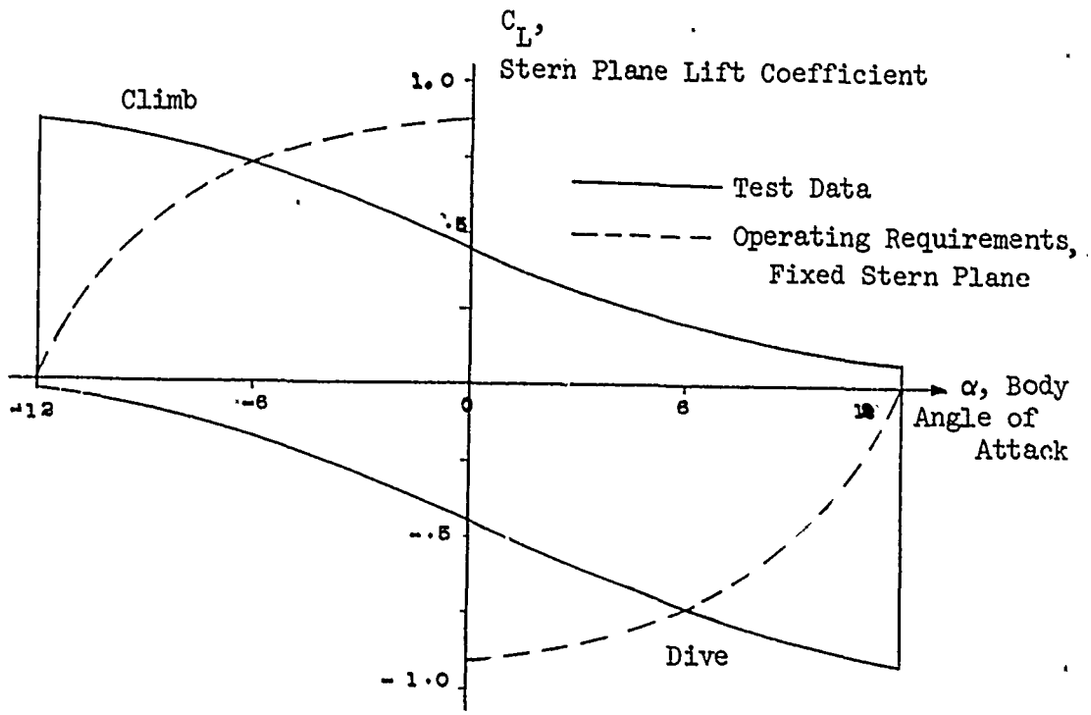

Figure 2 - Test Data and Operations Requirements

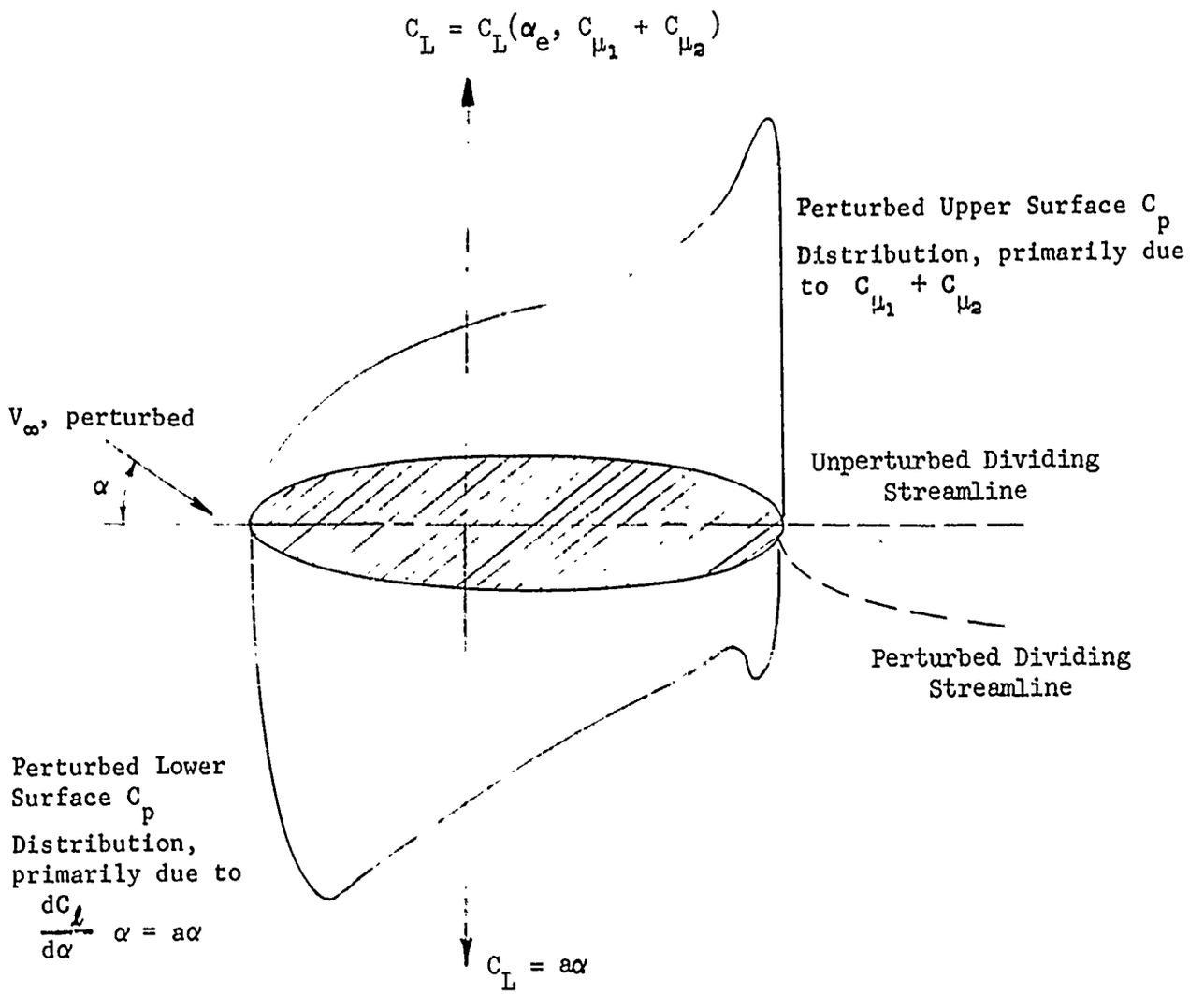

Figure 3 - Effect of Angle of Attack Perturbation on Stability With Equal Blowing from Upper and Lower Slots

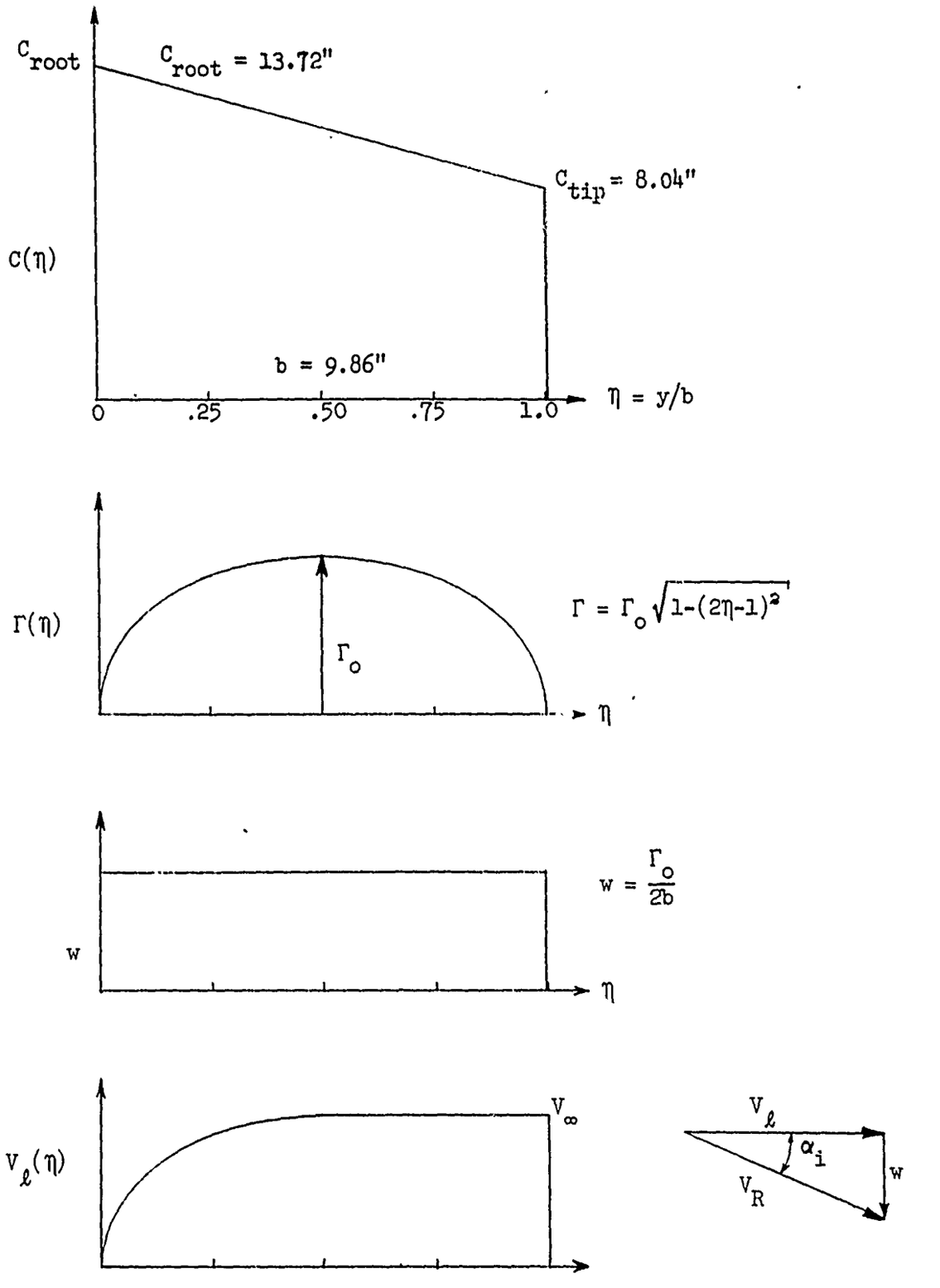

Figure 4 - Stern Plane Spanwise Distributions and Associated Nomenclature

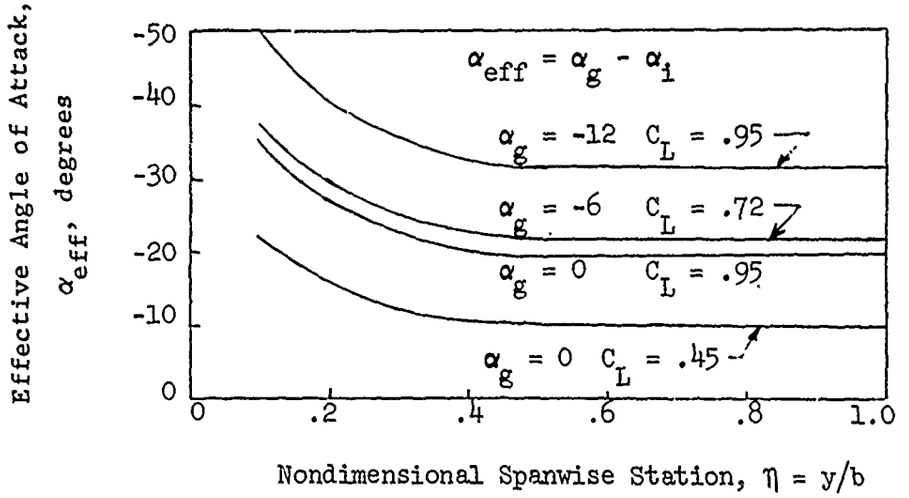

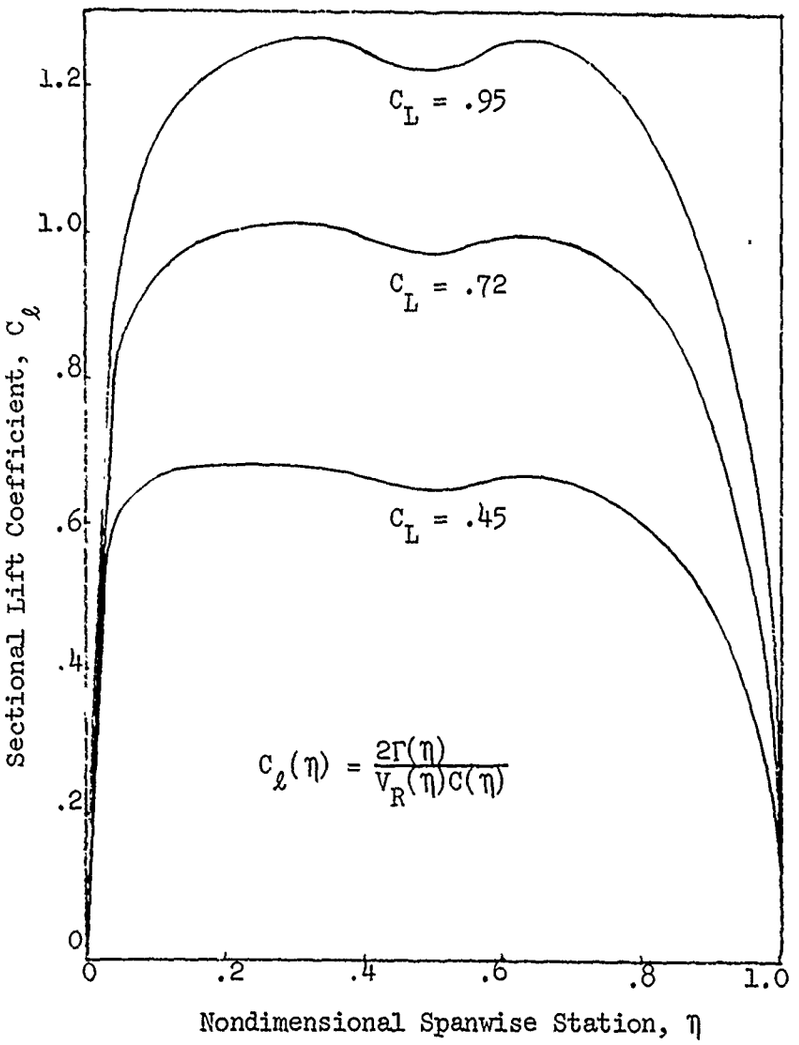

Figure 5 - Sectional Lift and Angle of Attack Distributions

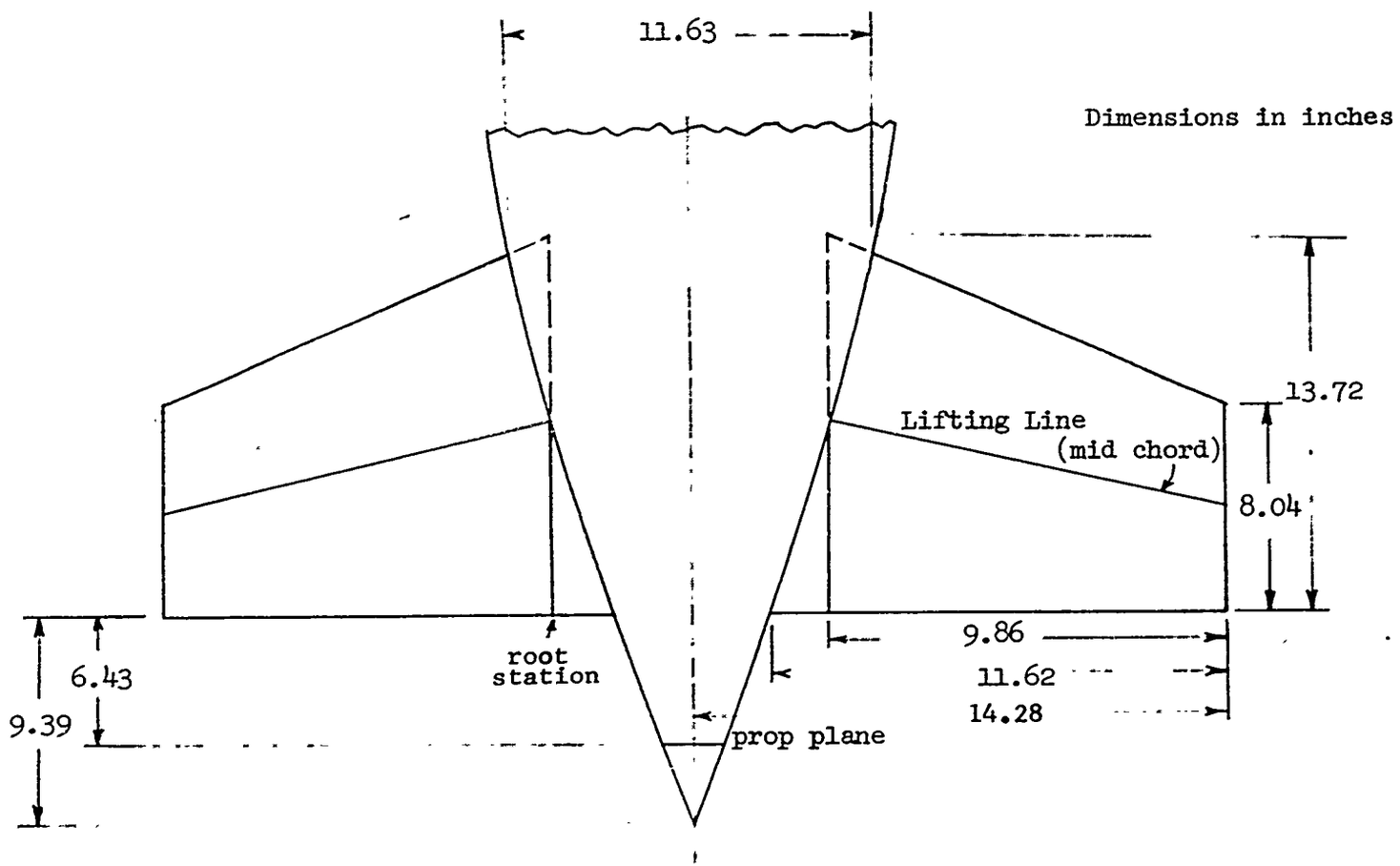

Figure 6 - Model Stern Plane Geometry

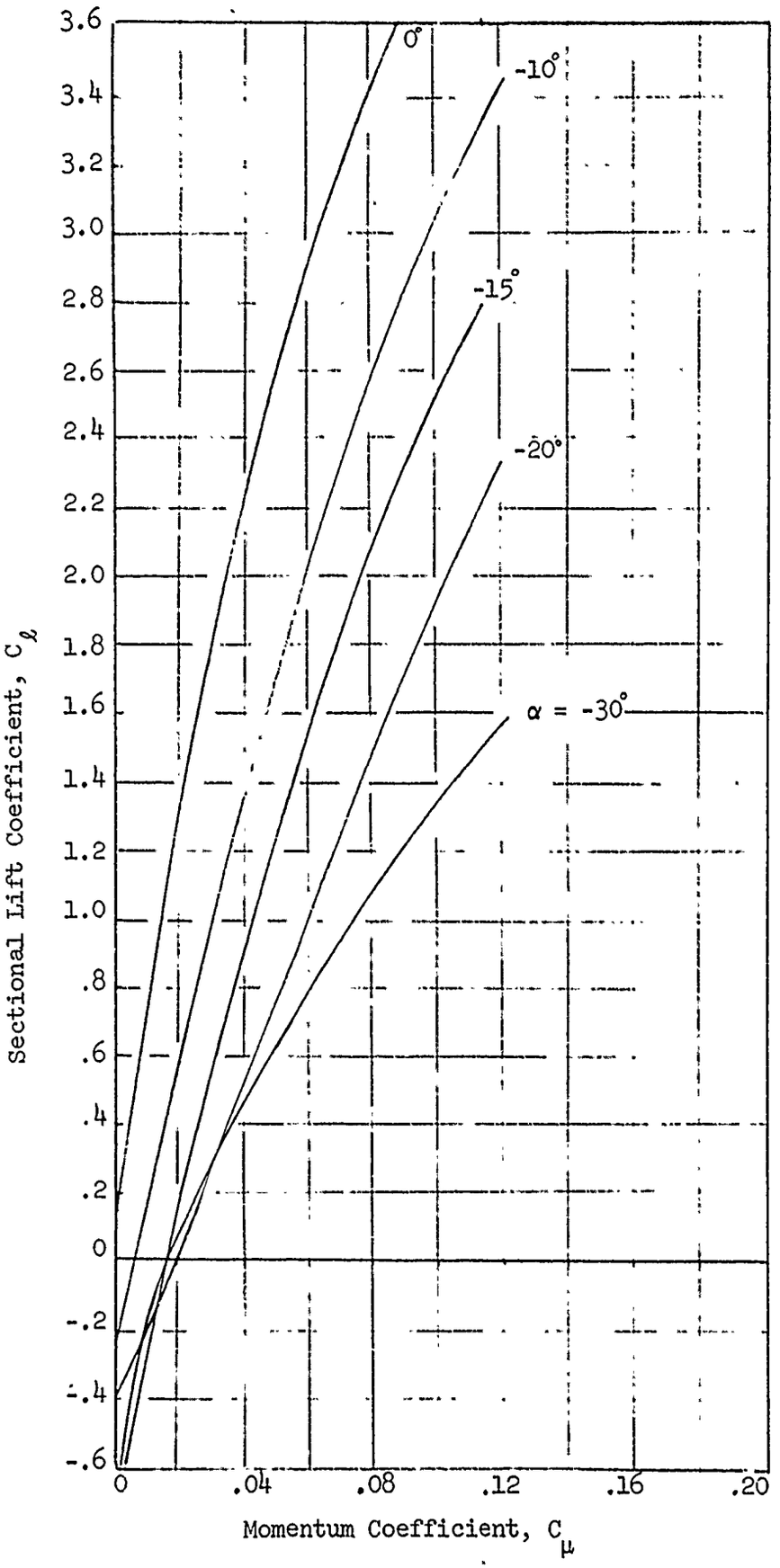

Figure 7 - Lift Characteristics for 30% Ellipse

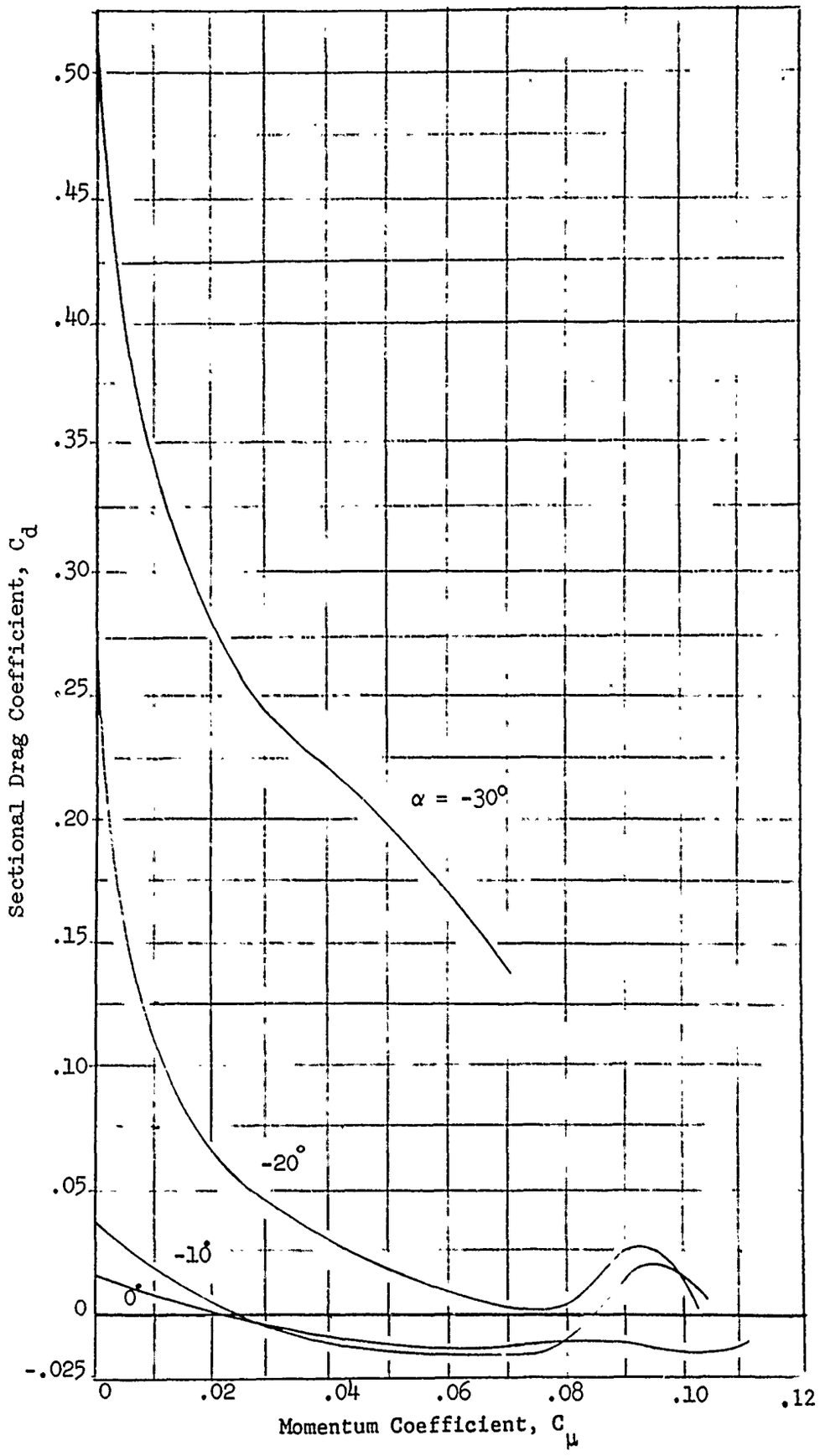

Figure 8 - Drag Characteristics for 30% Ellipse

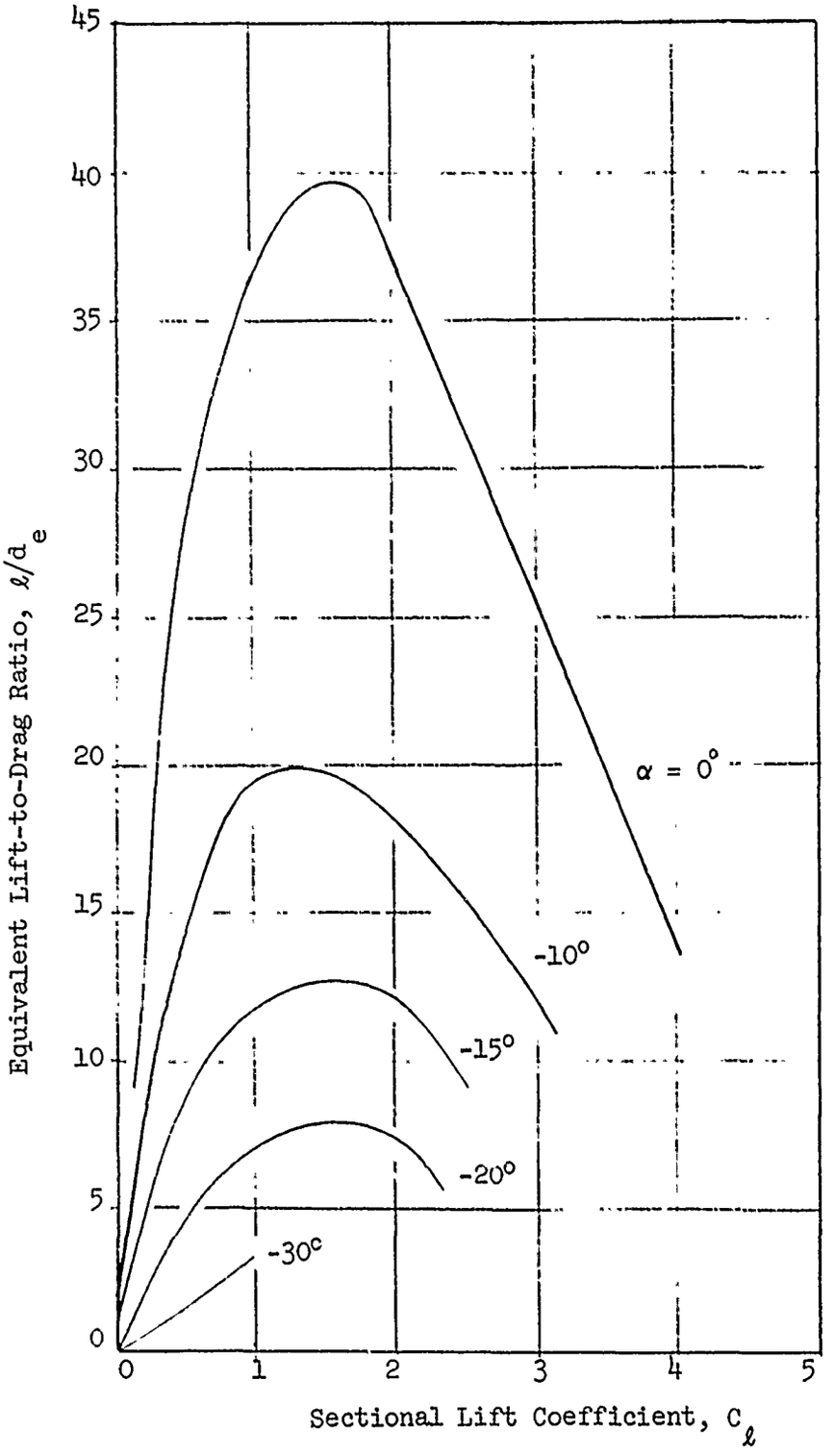

Figure 9 - Equivalent Lift-to-Drag Ratio for 30% Ellipse

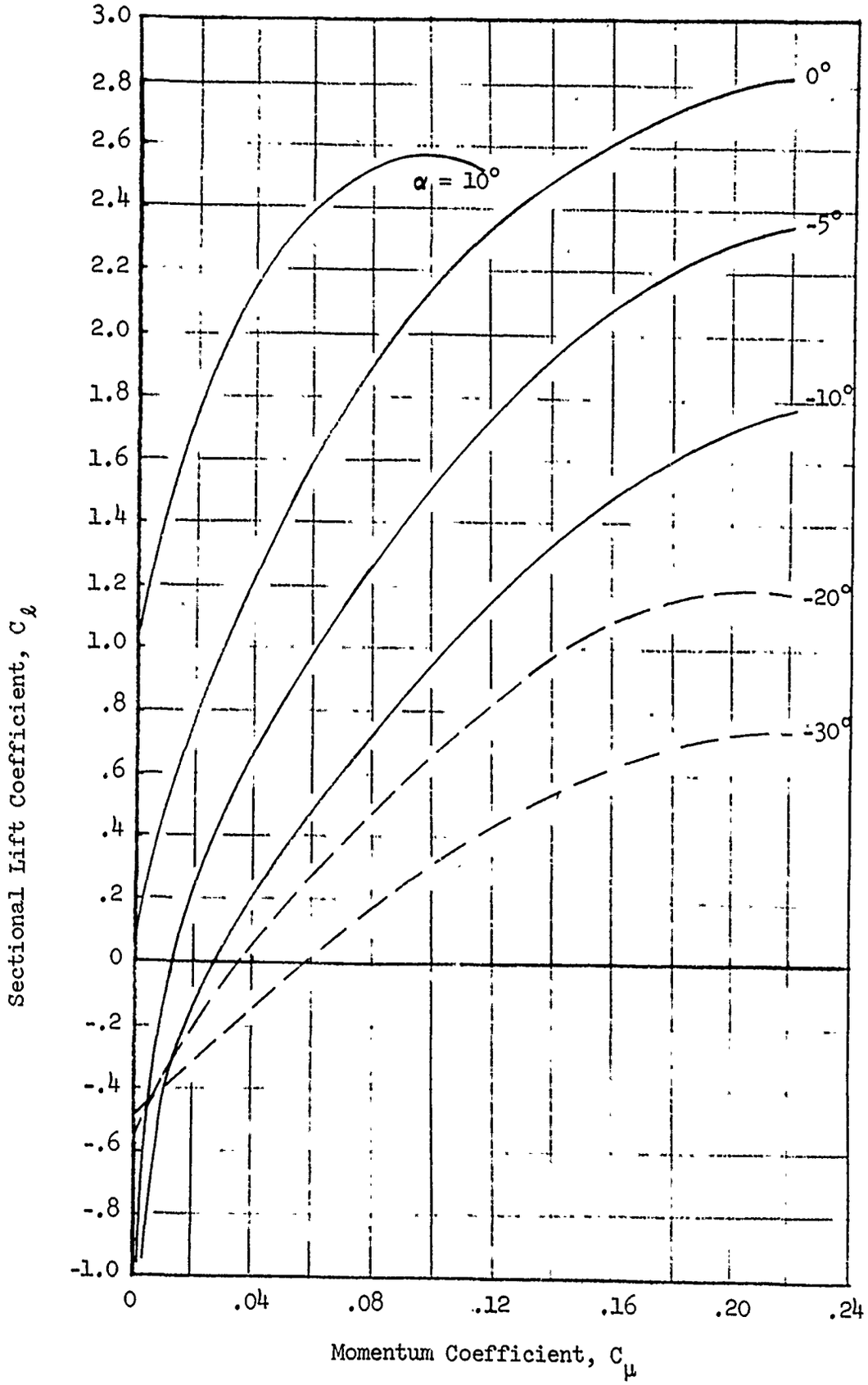

Figure 10 - Lift Characteristics for 20% Ellipse

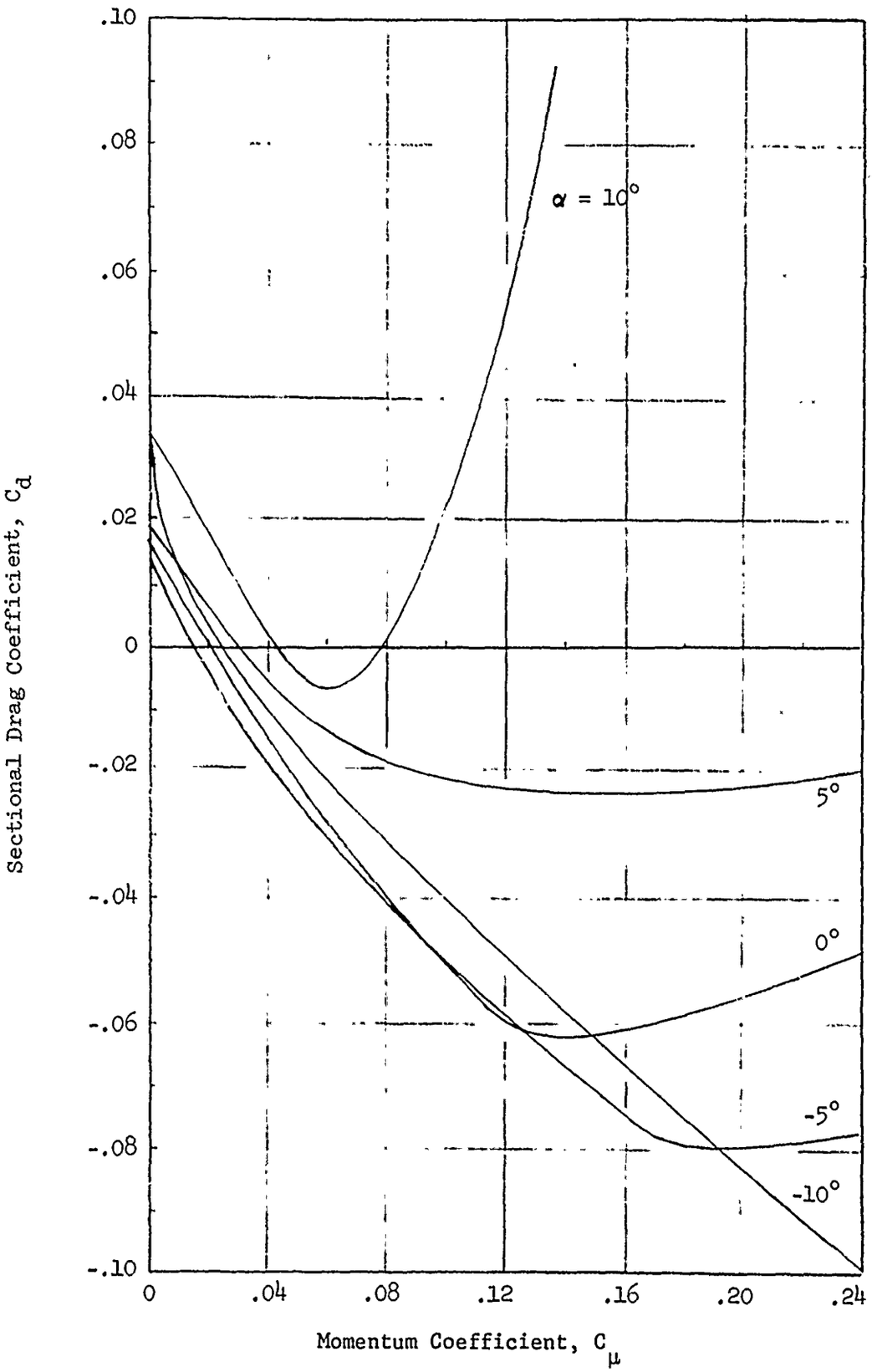

Figure 11 - Drag Characteristics for 20% Ellipse

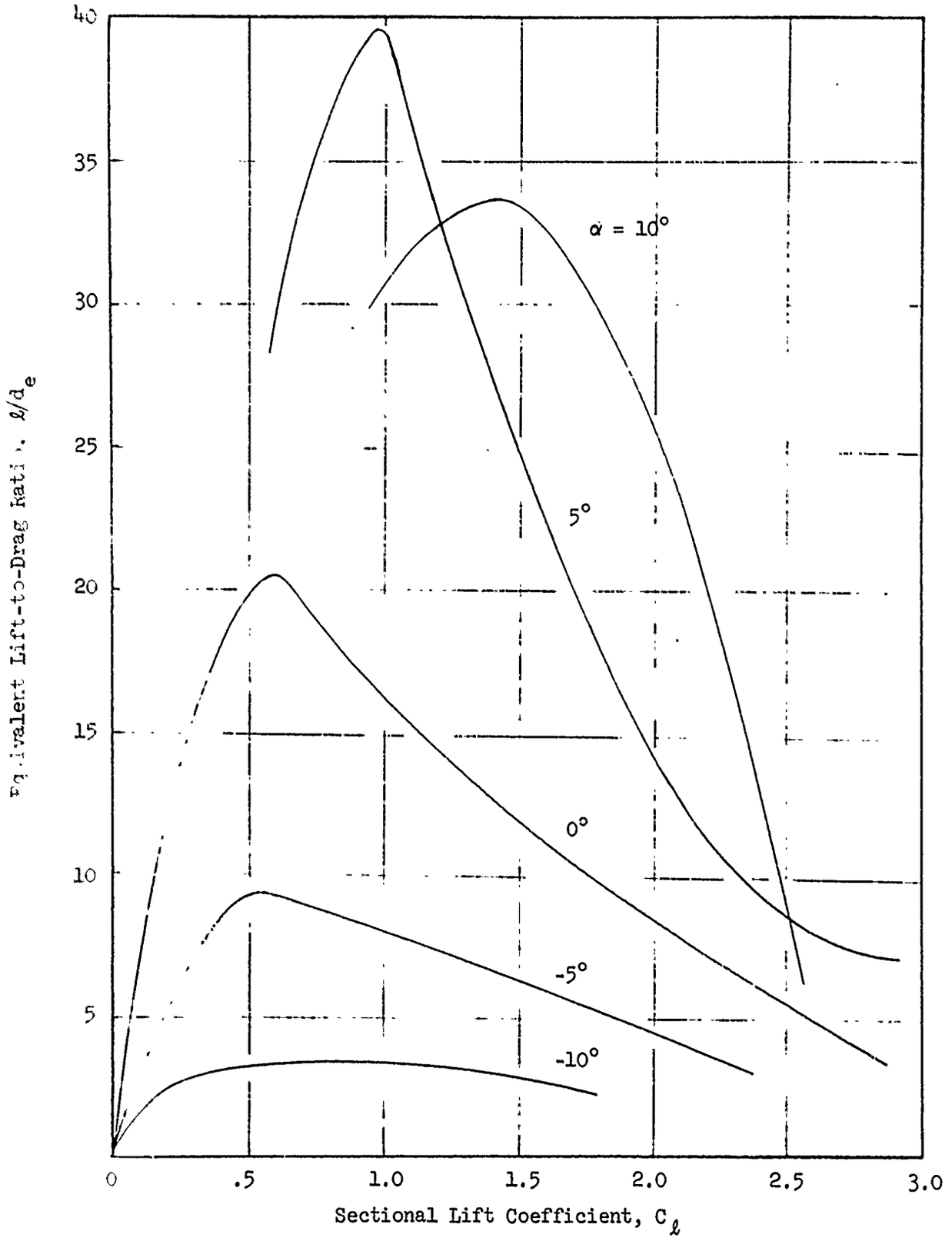

Figure 12 - Equivalent Lift-to-Drag Ratio for 20% Ellipse

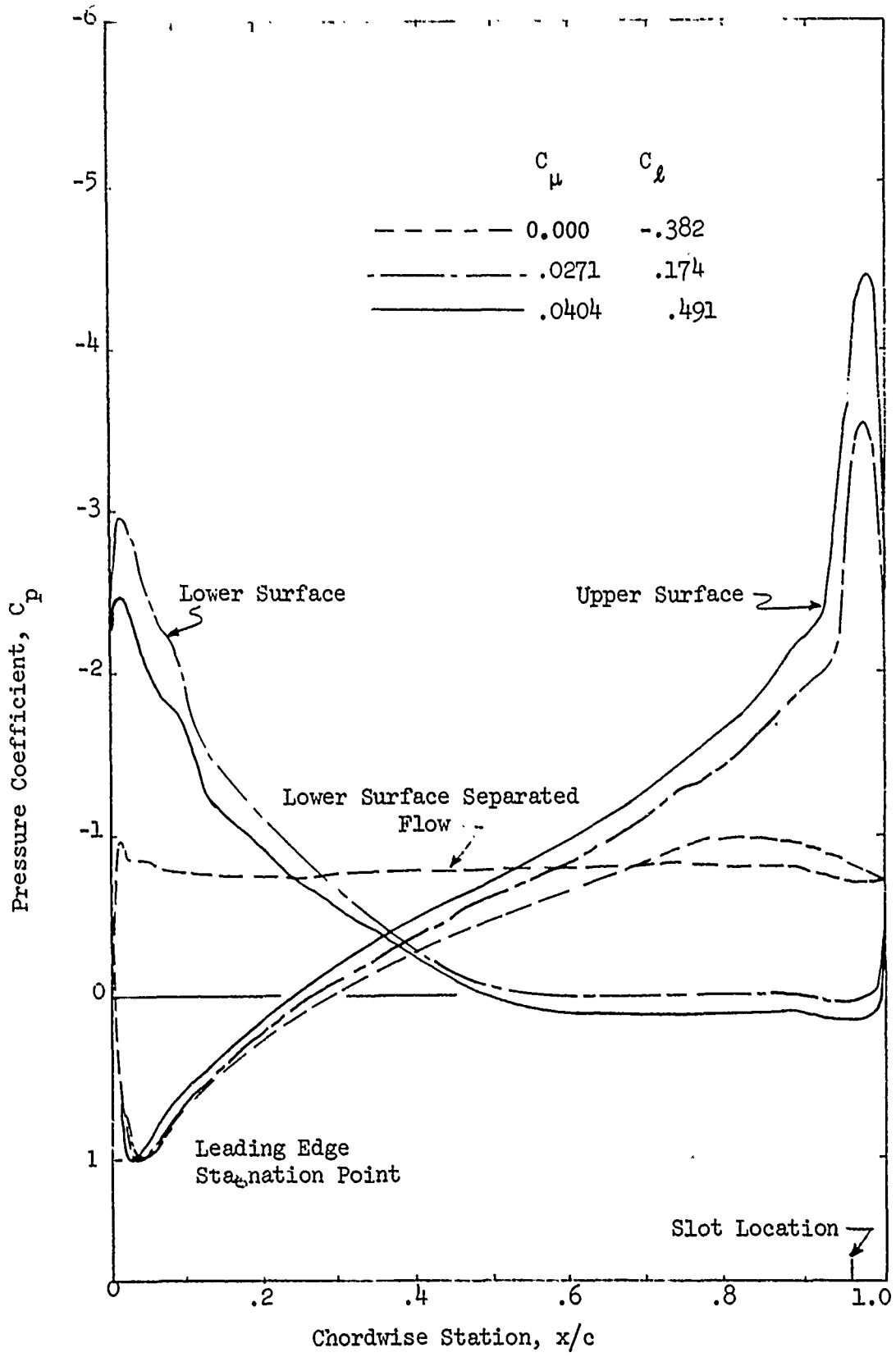

Figure 13 - Experimental Pressure Distributions for 30% Ellipse at $\alpha = -20°$

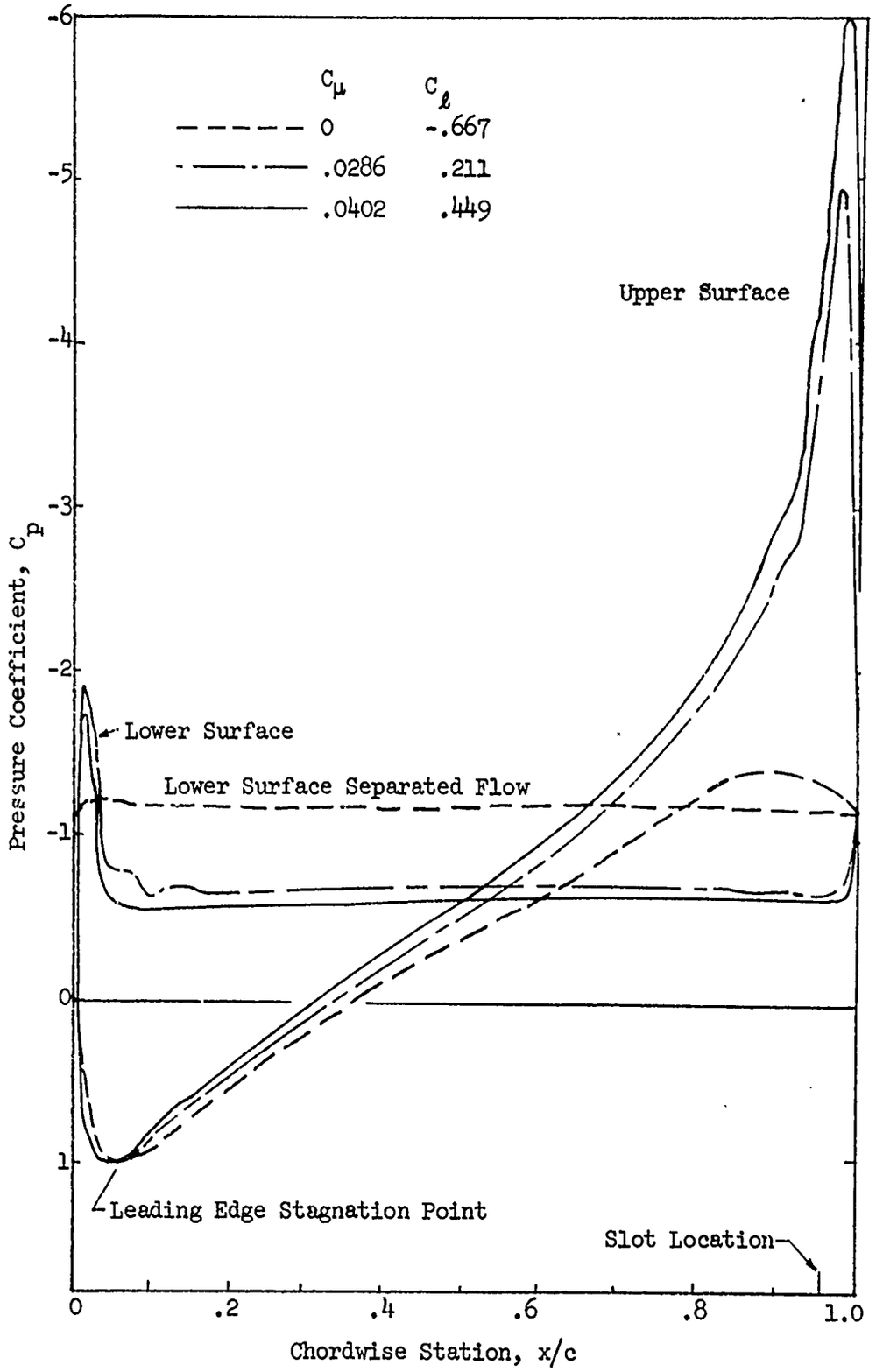

Figure 14 - Experimental Pressure Distribution for 30% Ellipse at $\alpha = -30°$

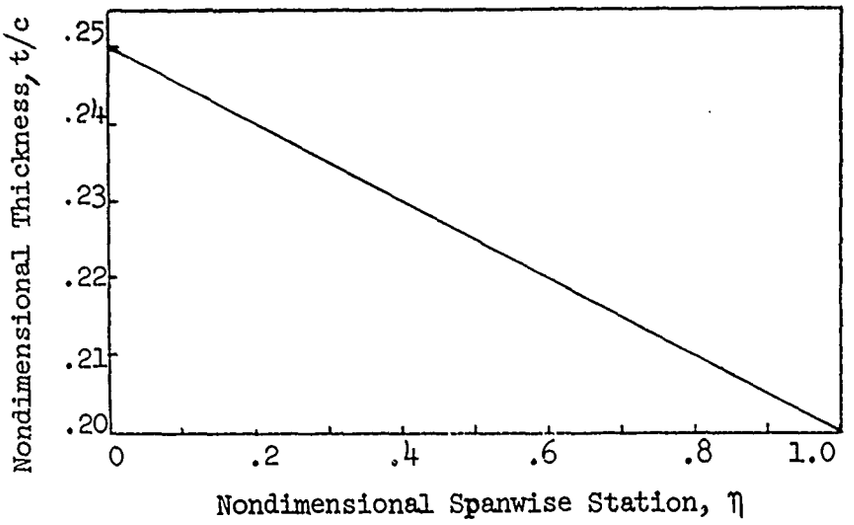

Figure 15 - Design Thickness Distribution

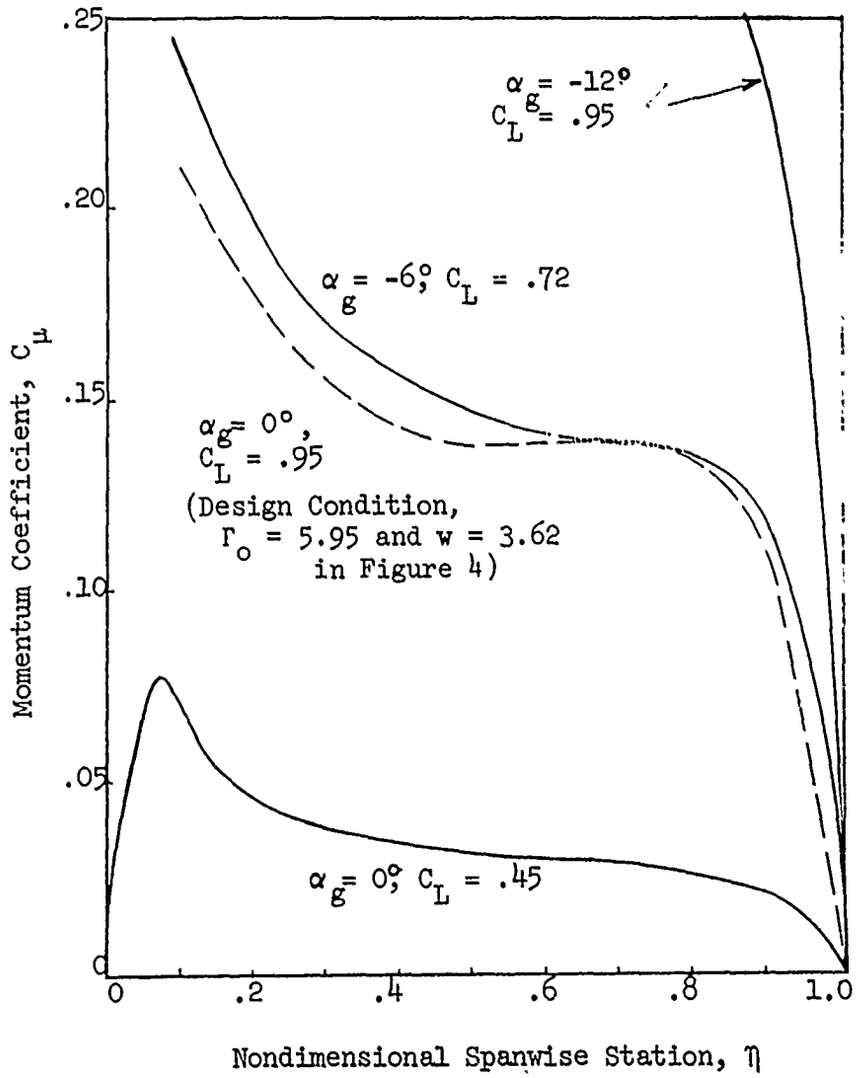

Figure 16 - Spanwise Momentum Coefficient Requirements

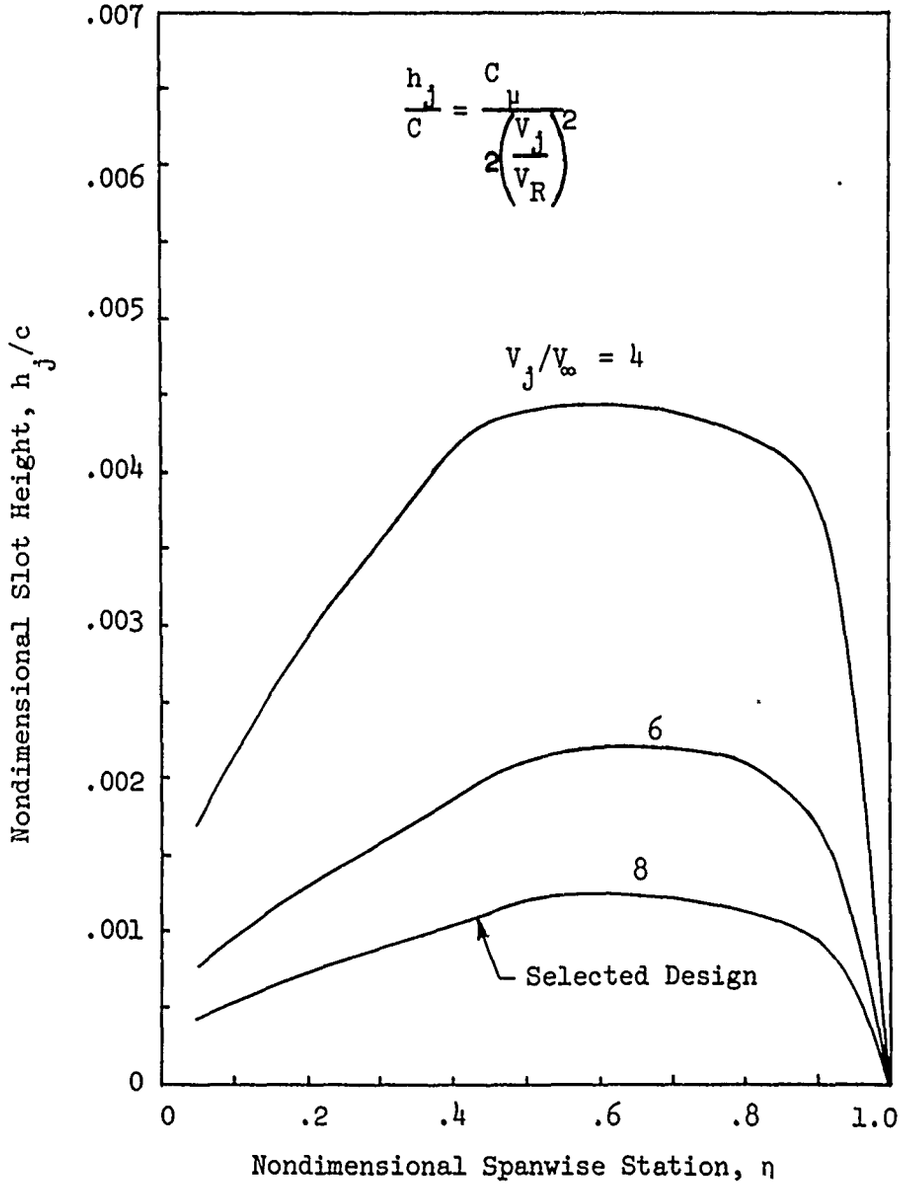

Figure 17 - Nondimensional Slot Height Requirements for Design Condition

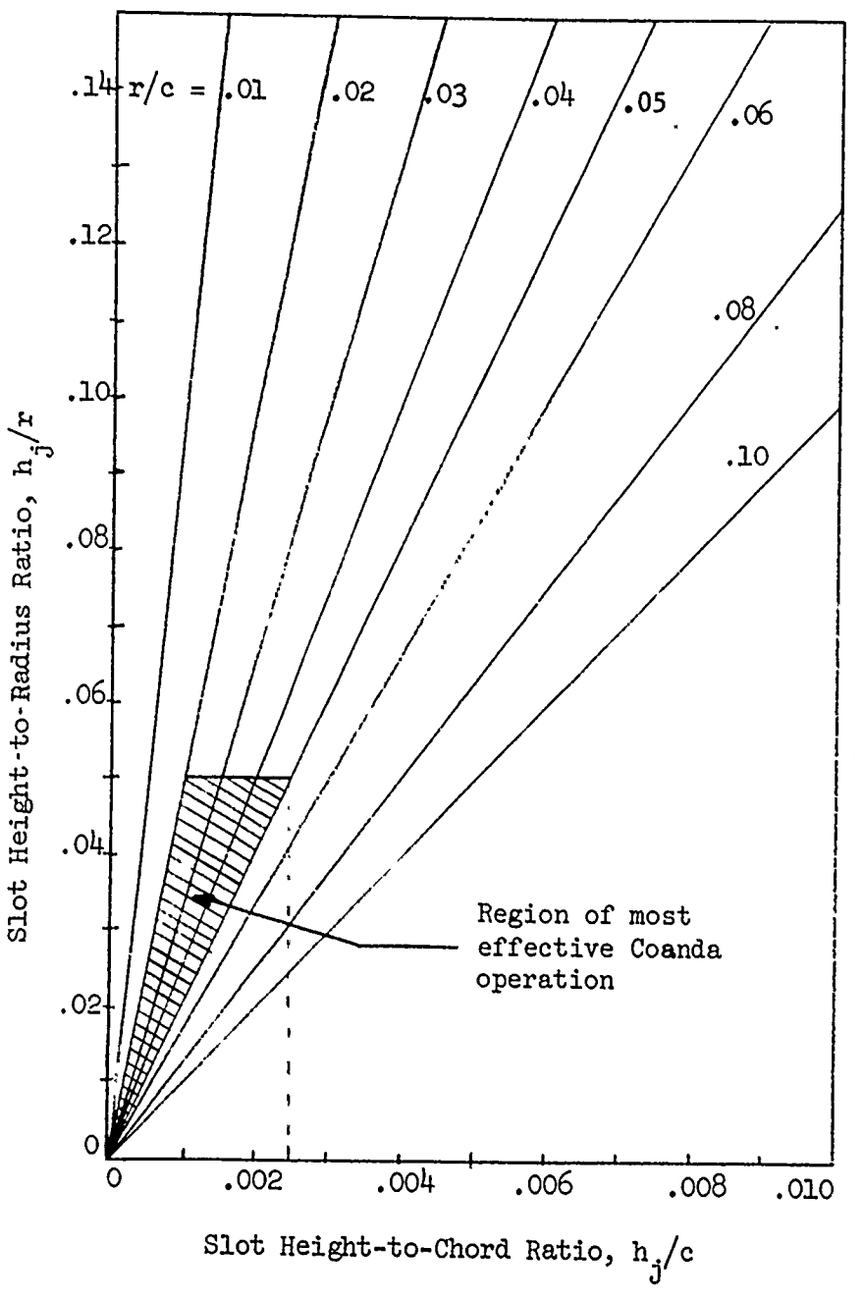

Figure 18 - Dimensionless Slot Height and Trailing Edge Radius Relationships

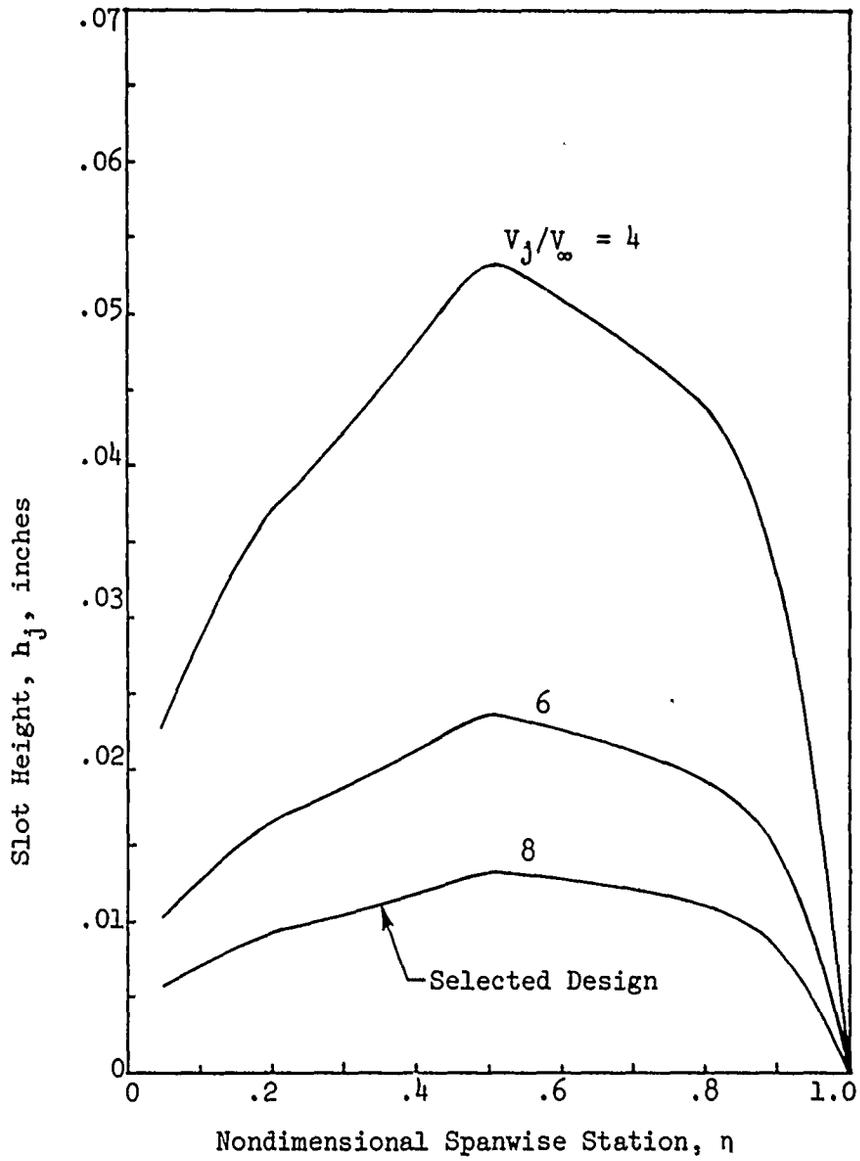

Figure 19 - Slot Height Requirements for the Design Condition

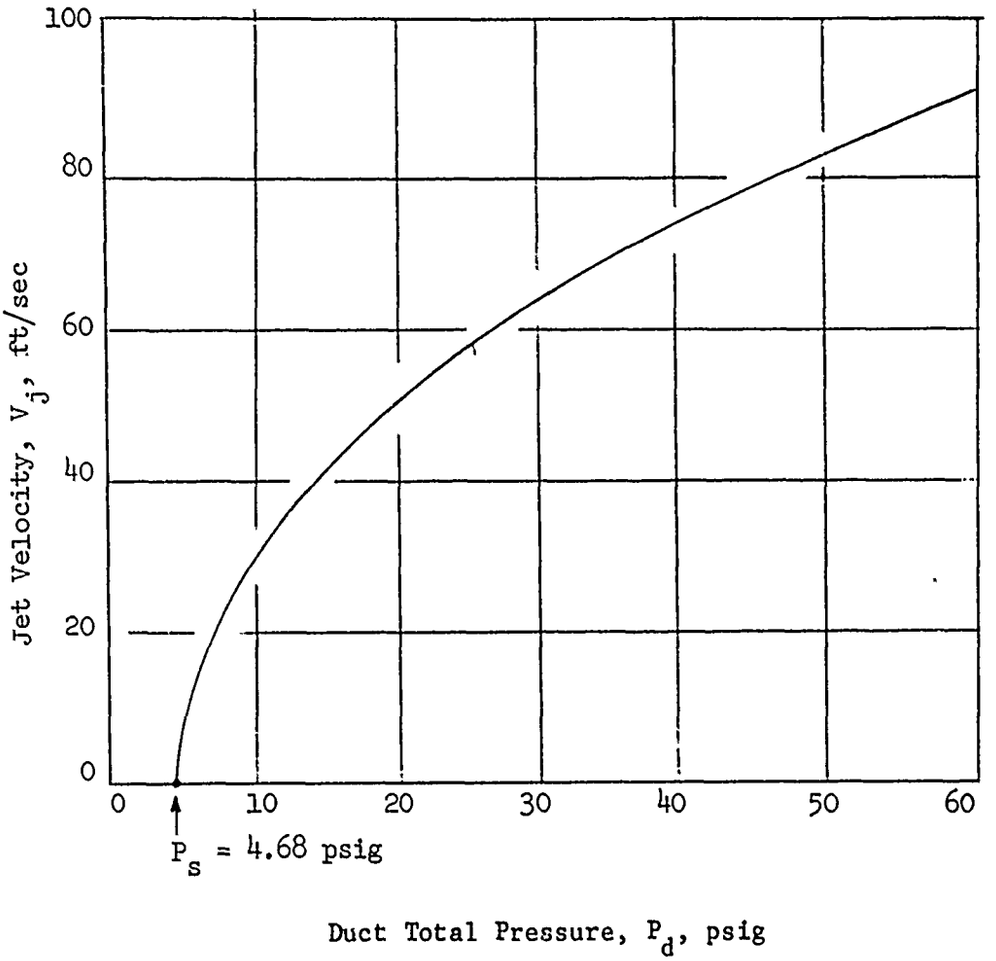

Figure 20 - Jet Velocity at Eleven Feet of Depth

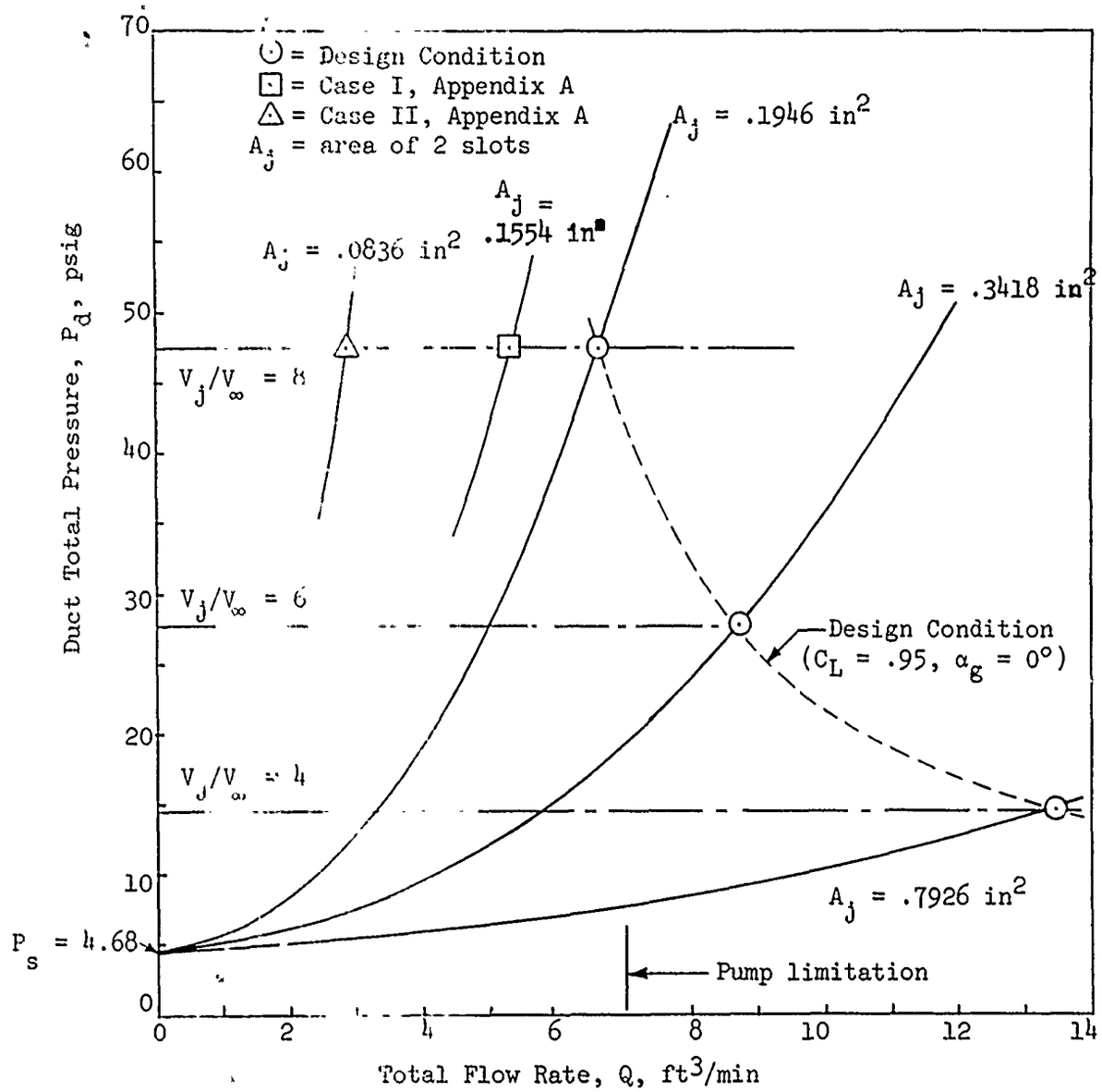

Figure 21 - Total Flow Rate for the Design Condition
(V_∞ = 10.2 ft/sec)

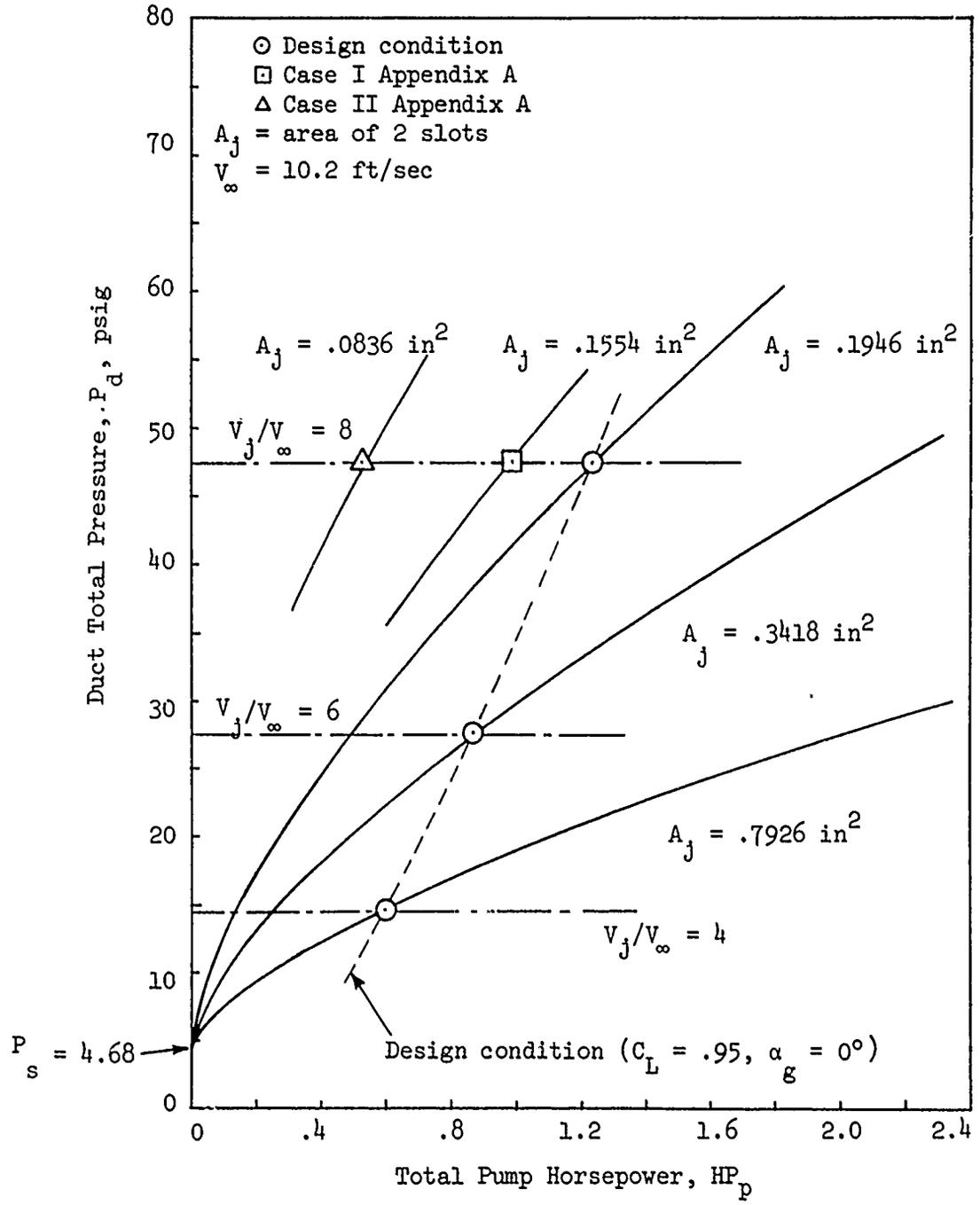

Figure 22 - Power Requirements for the Design Condition

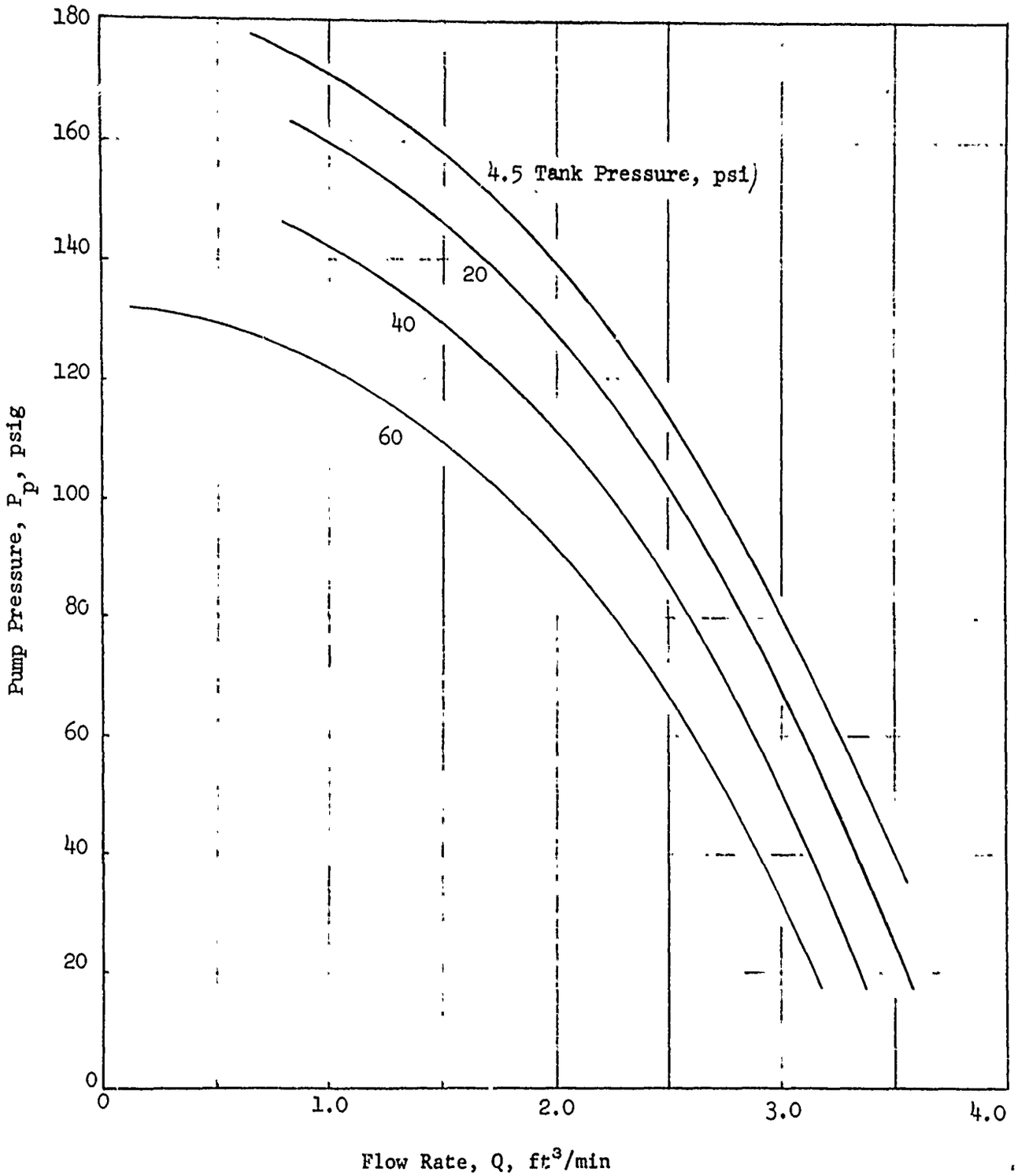

Figure 23 - Characteristics of the Crane 7- AHF4 Pump

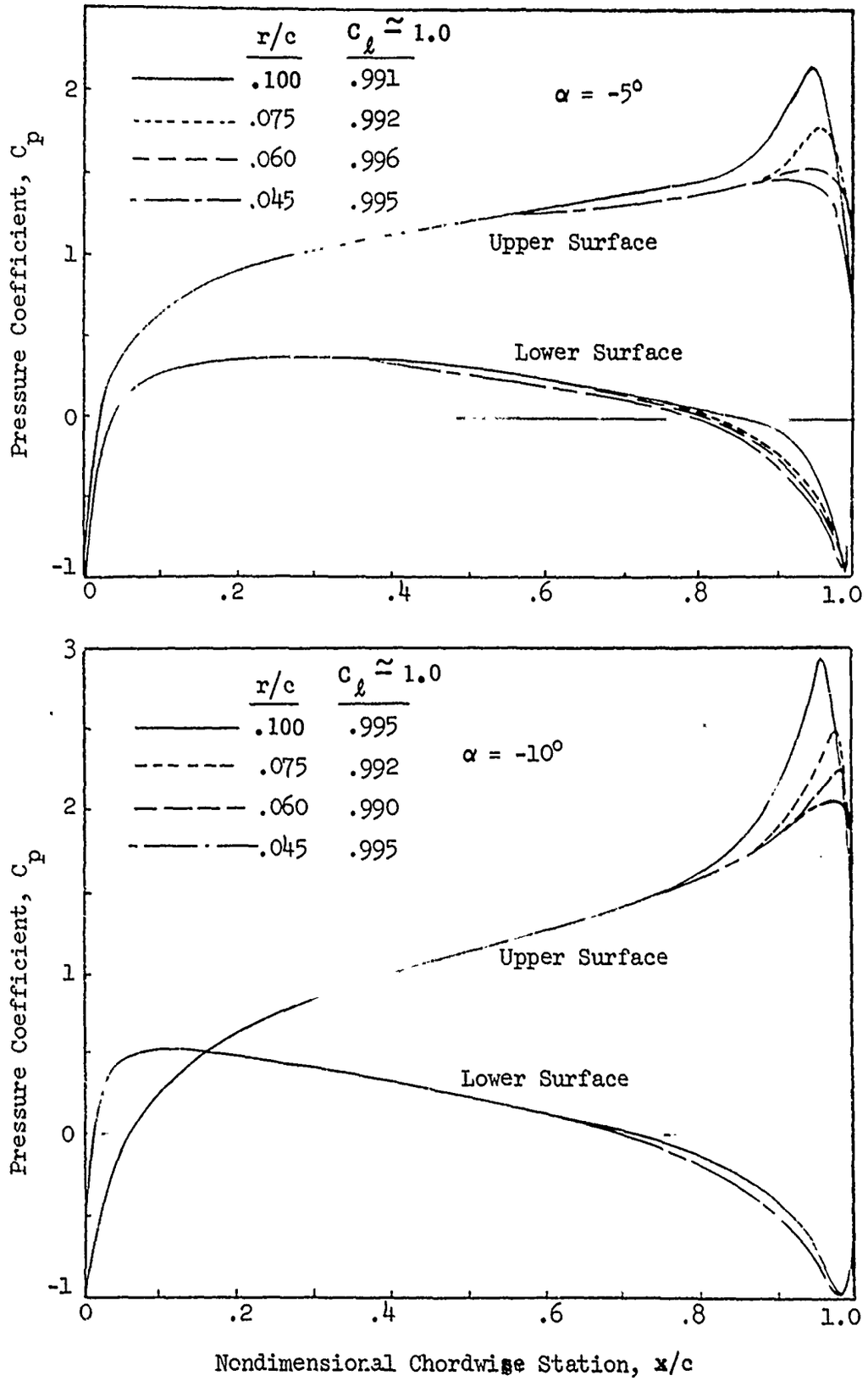

Figure 24 - Variation in Potential Flow Pressure Distributions With Change in Trailing Edge Radius on 30% Ellipse With 1.25% Camber

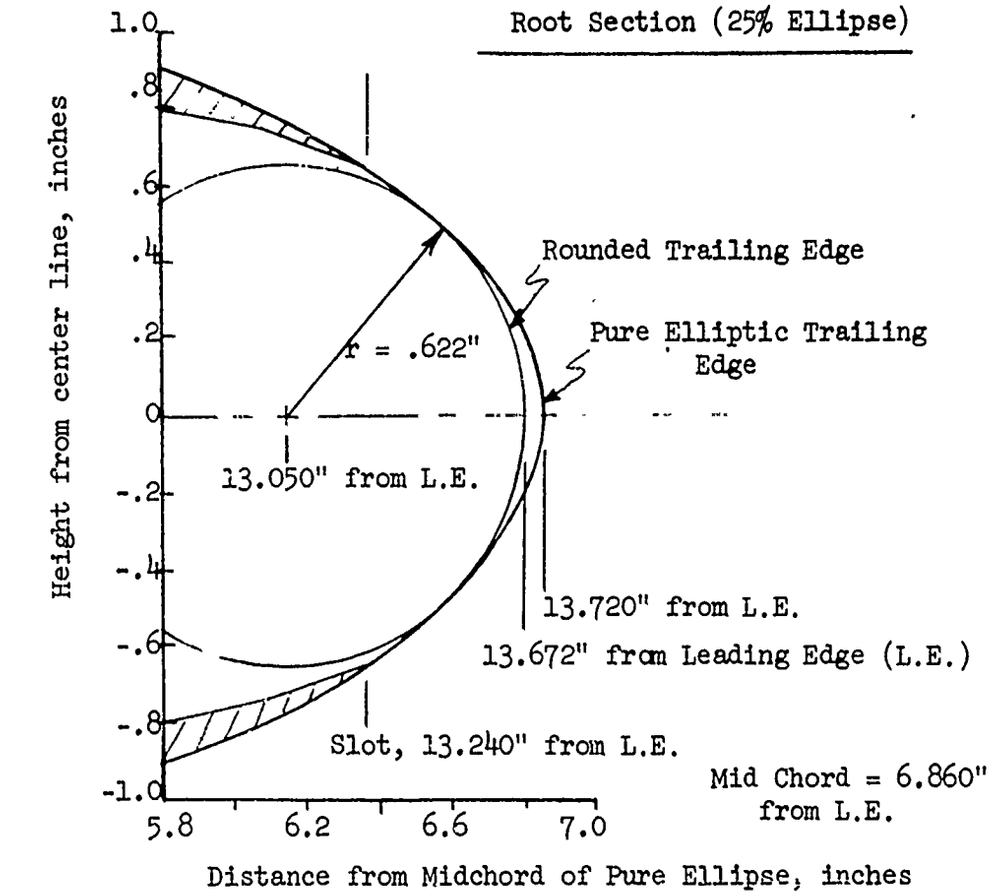

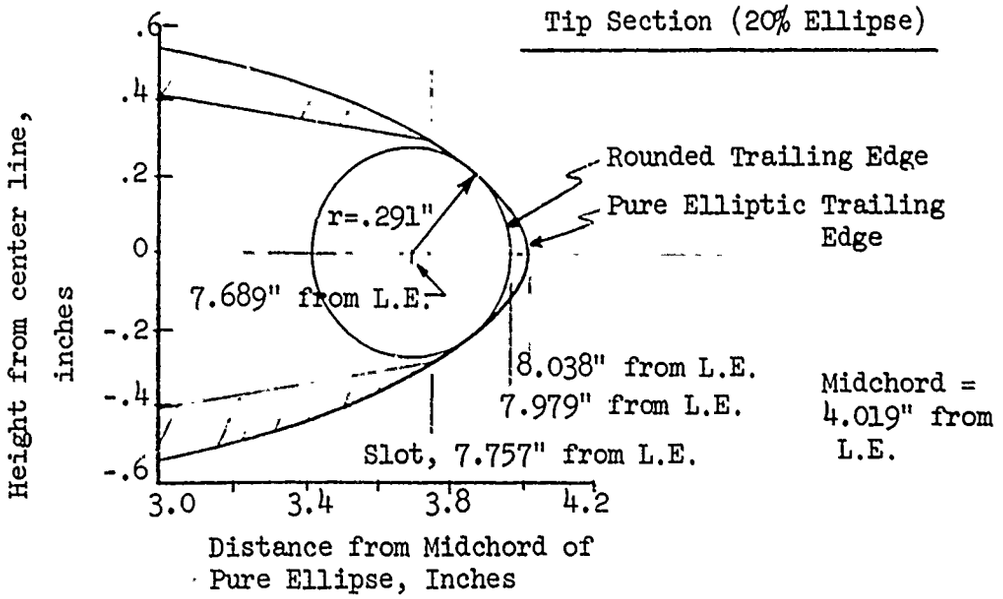

Figure 25 ~ Trailing Edge Detail

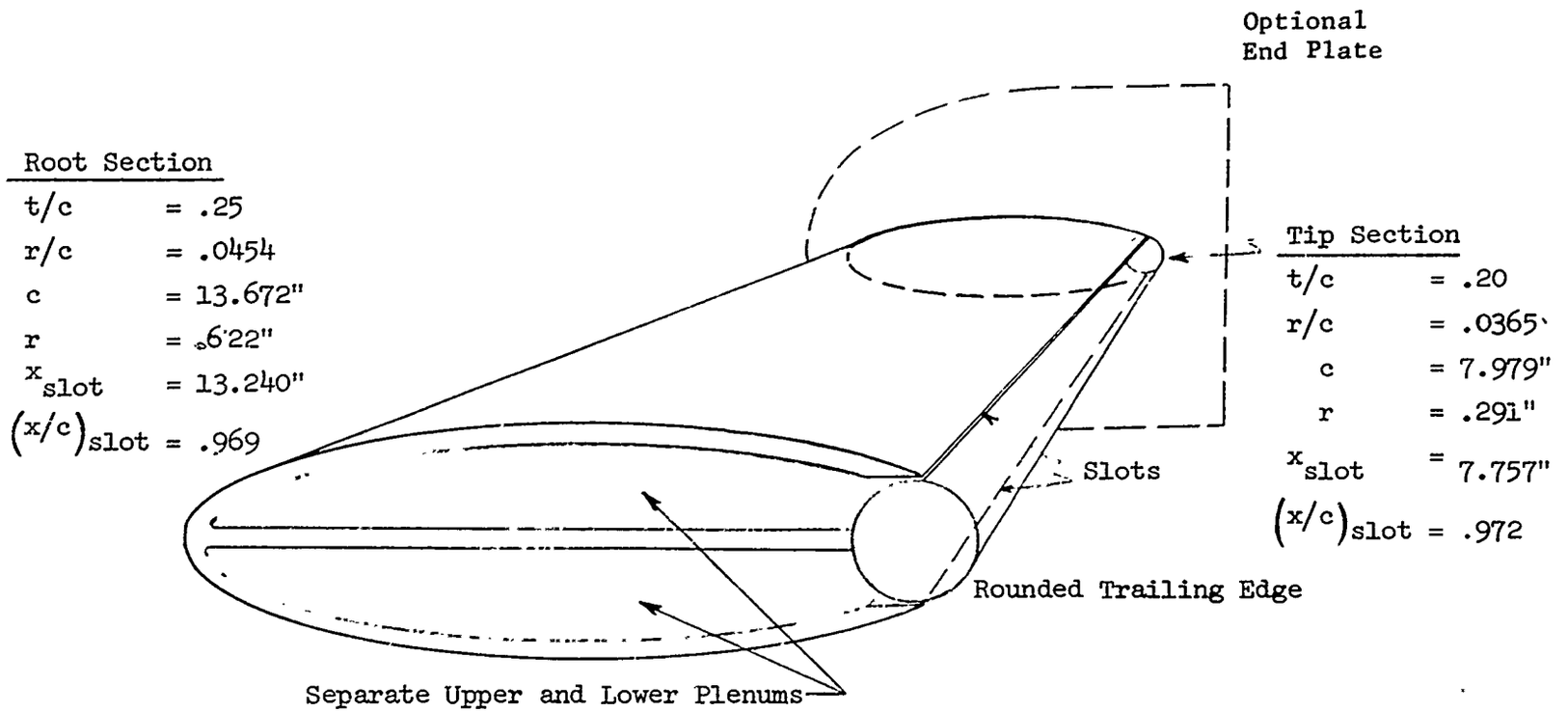

Figure 26 - Blown Model Stern Plane Design

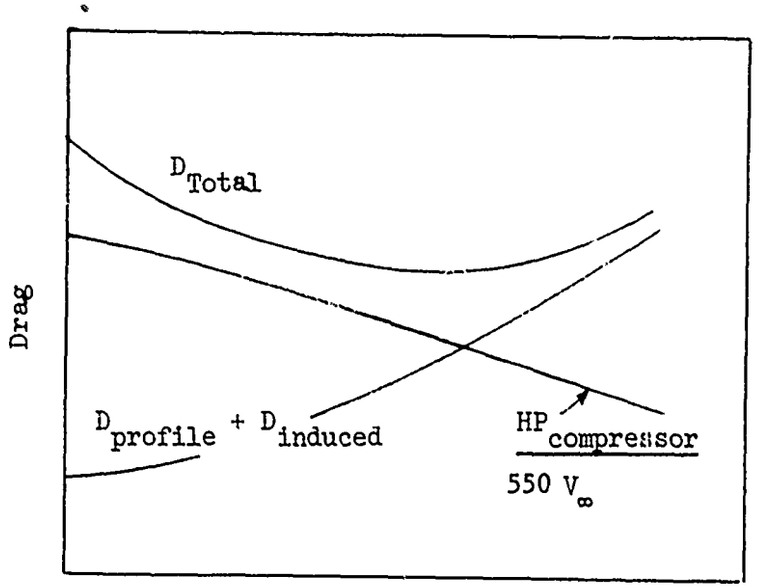

End Plate Height-to-Span Ratio H/b

Figure 27 - Tradeoff Between End Plate Drag Increase And Compressor Power Reduction

$$\frac{H}{b} = K_o + K_\mu = \frac{2h}{b}$$

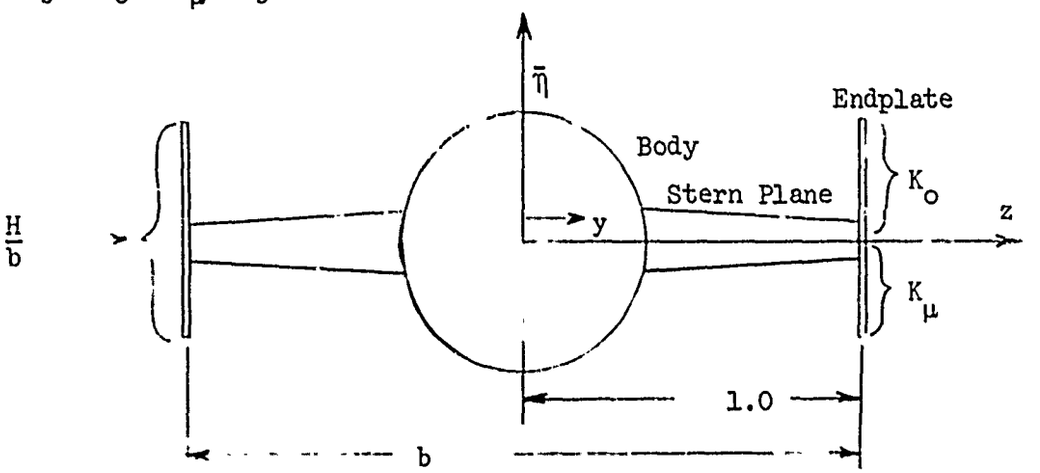

Figure 28 - End Plate Nomenclature

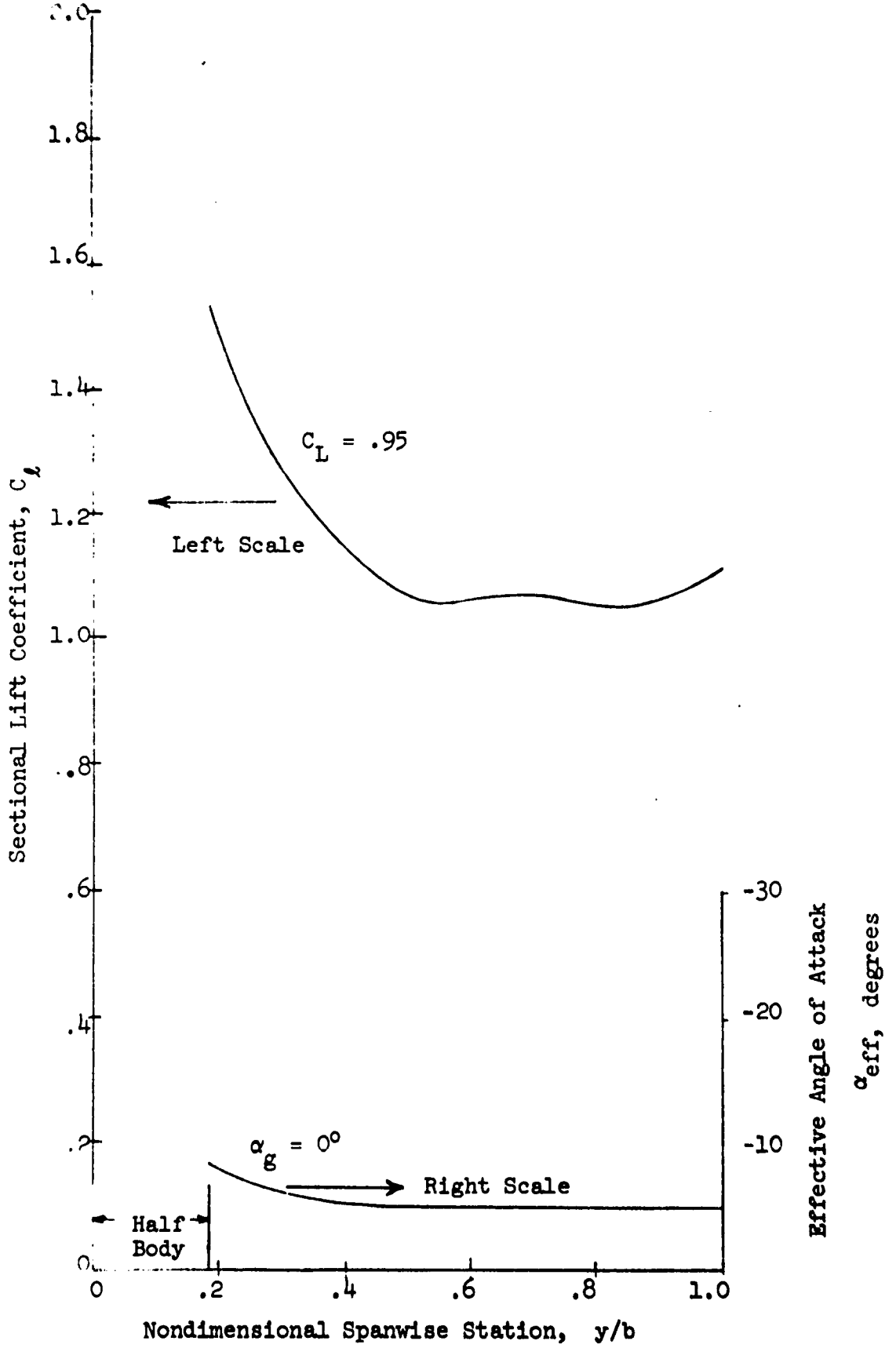

Figure 29 - Lift Coefficient and Angle of Attack Distributions for Endplated Configuration

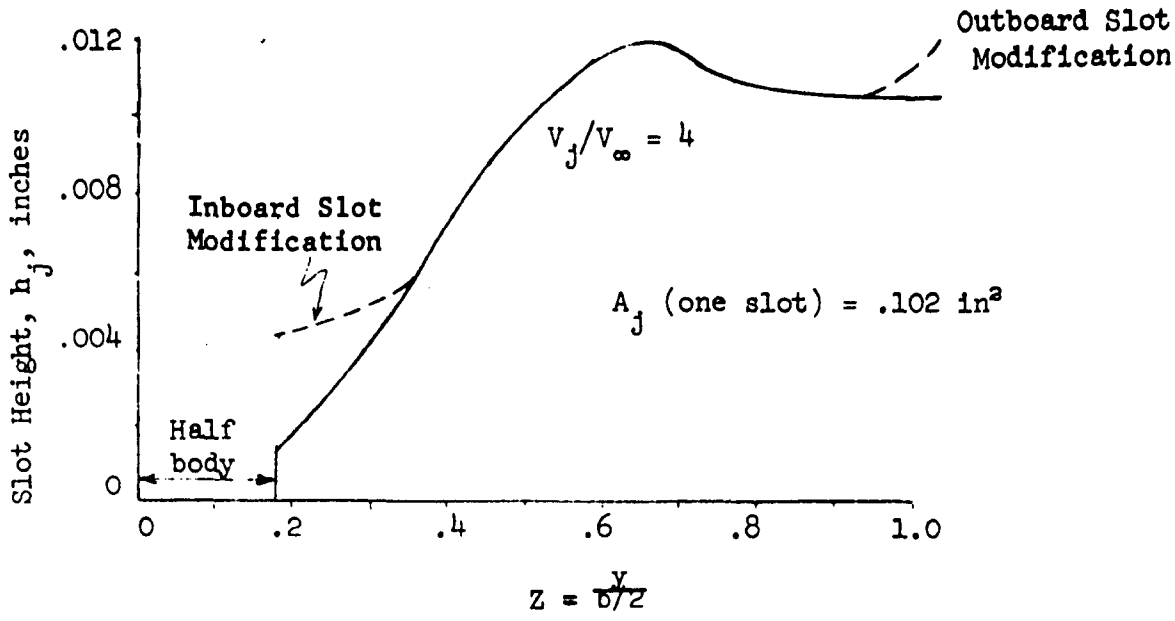

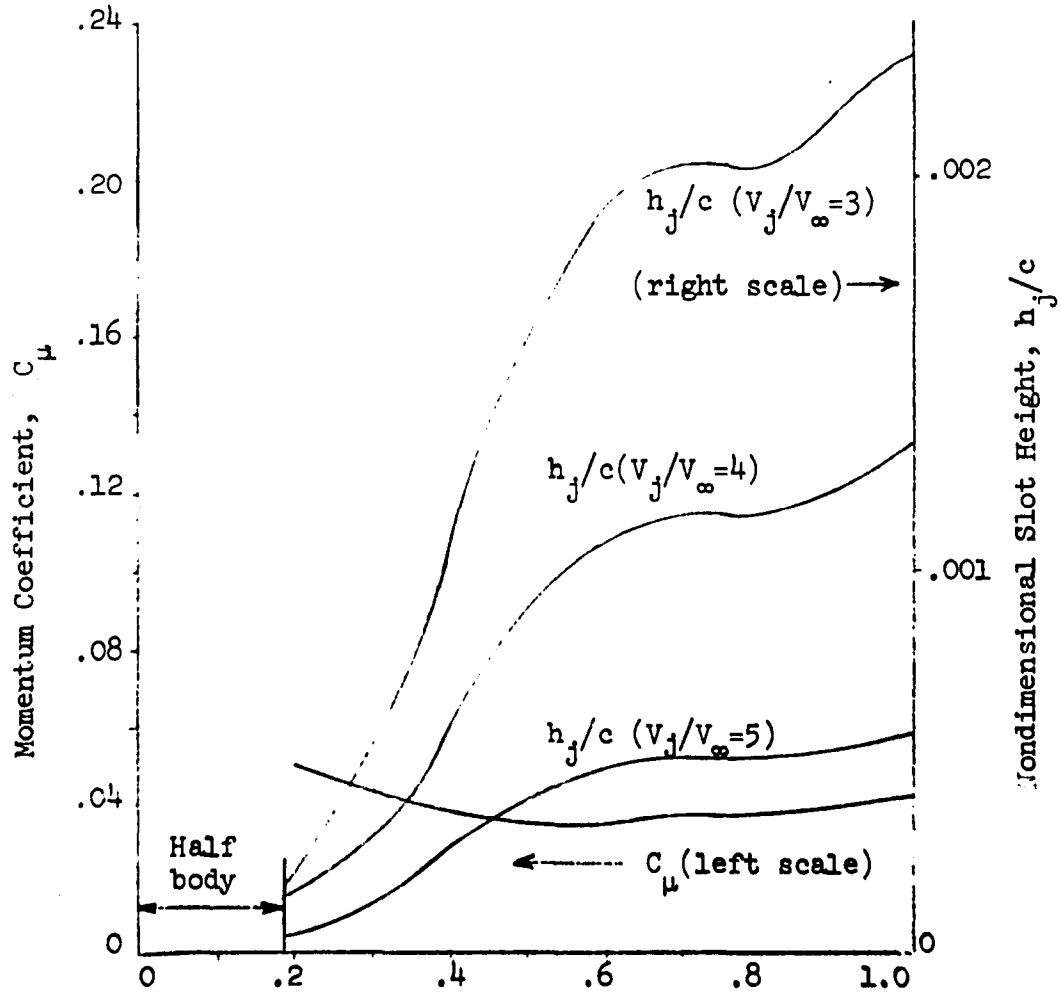

Figure 30 - Slot Height and Momentum Coefficient For Endplated Configuration

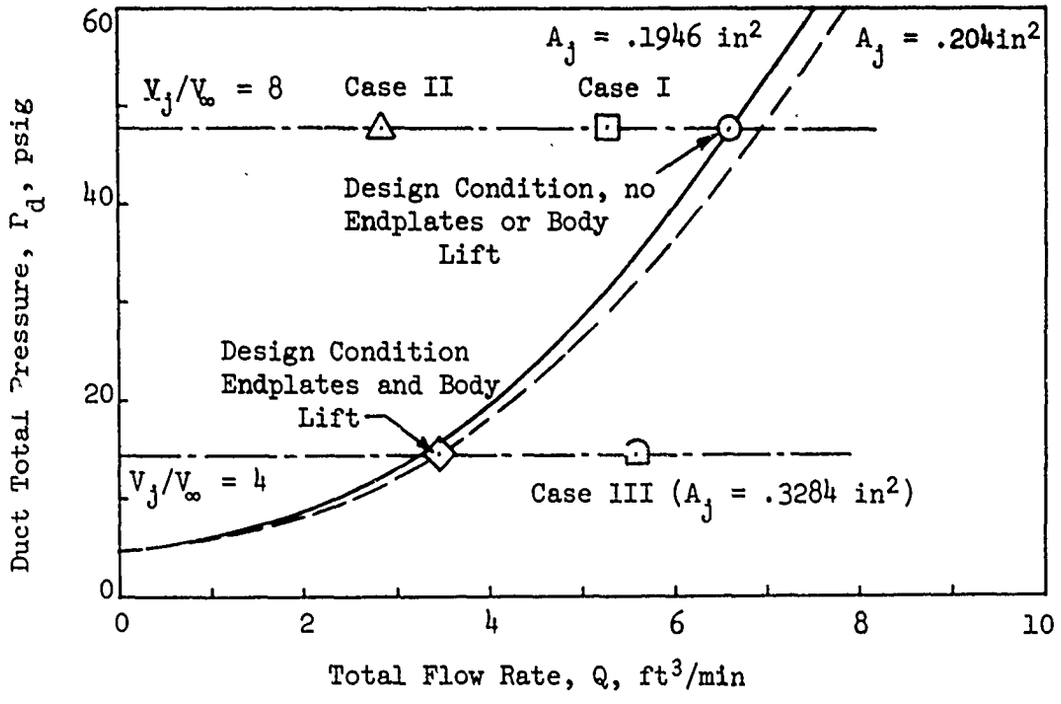

(Cases I, II, and III from Appendix A)

Design Condition: C_L = .95, α_g = 0°, V_∞ = 10.2 ft/sec.

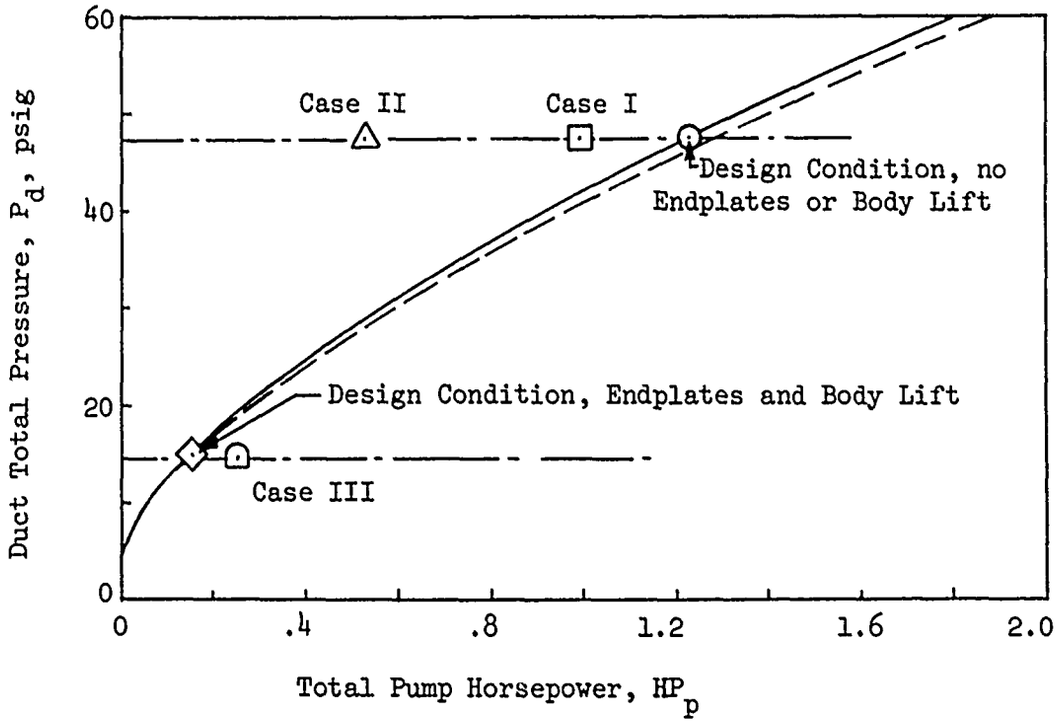

Figure 31 - Effect of Endplates on Design Condition Power and Flow Rate Requirements

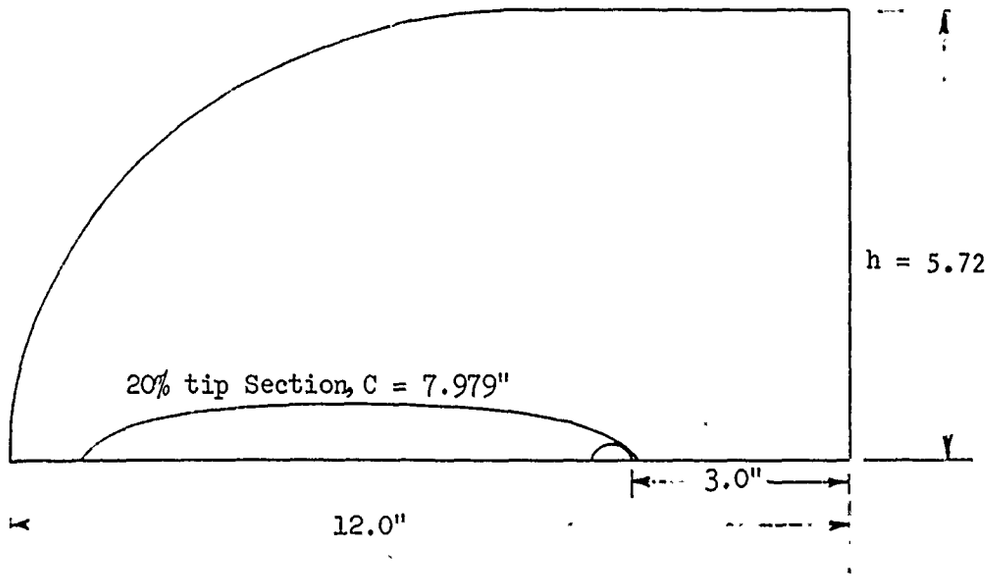

Figure 32 - Model End Plate Geometry

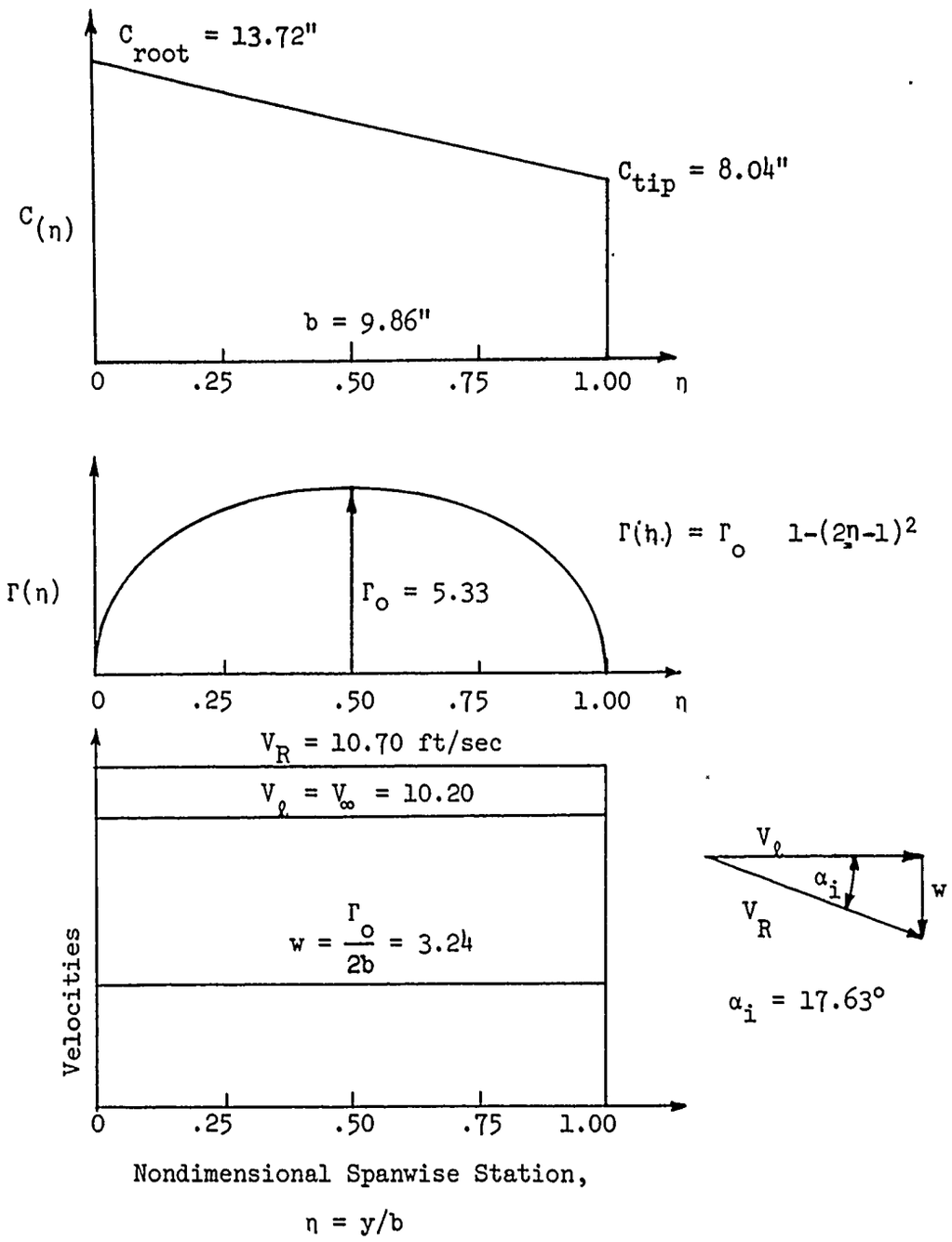

Figure 33 - Spanwise Distributions for Case I

(Simplified Velocity Assumption)

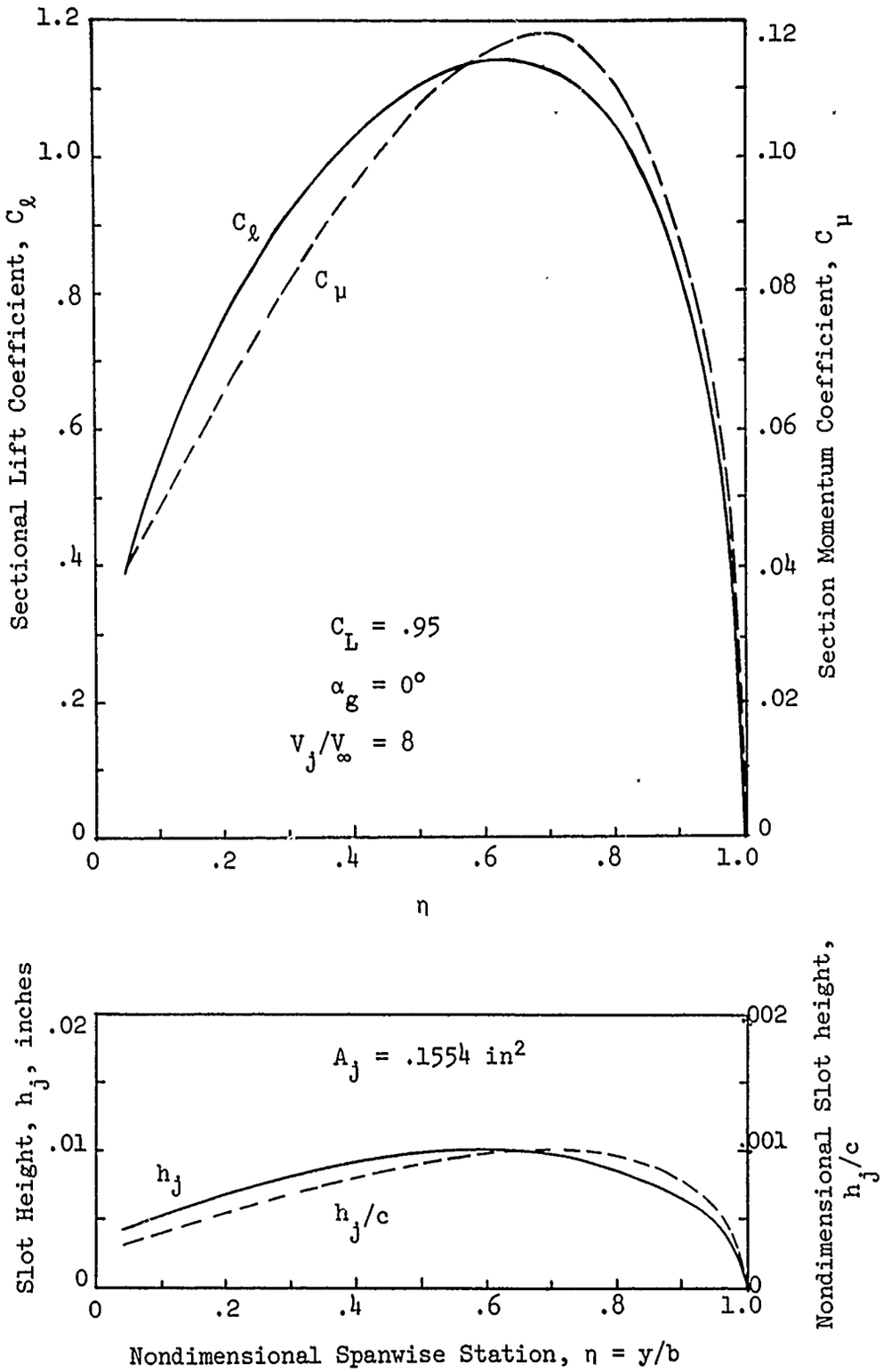

Figure 34 - Resulting Spanwise Distributions for Case I

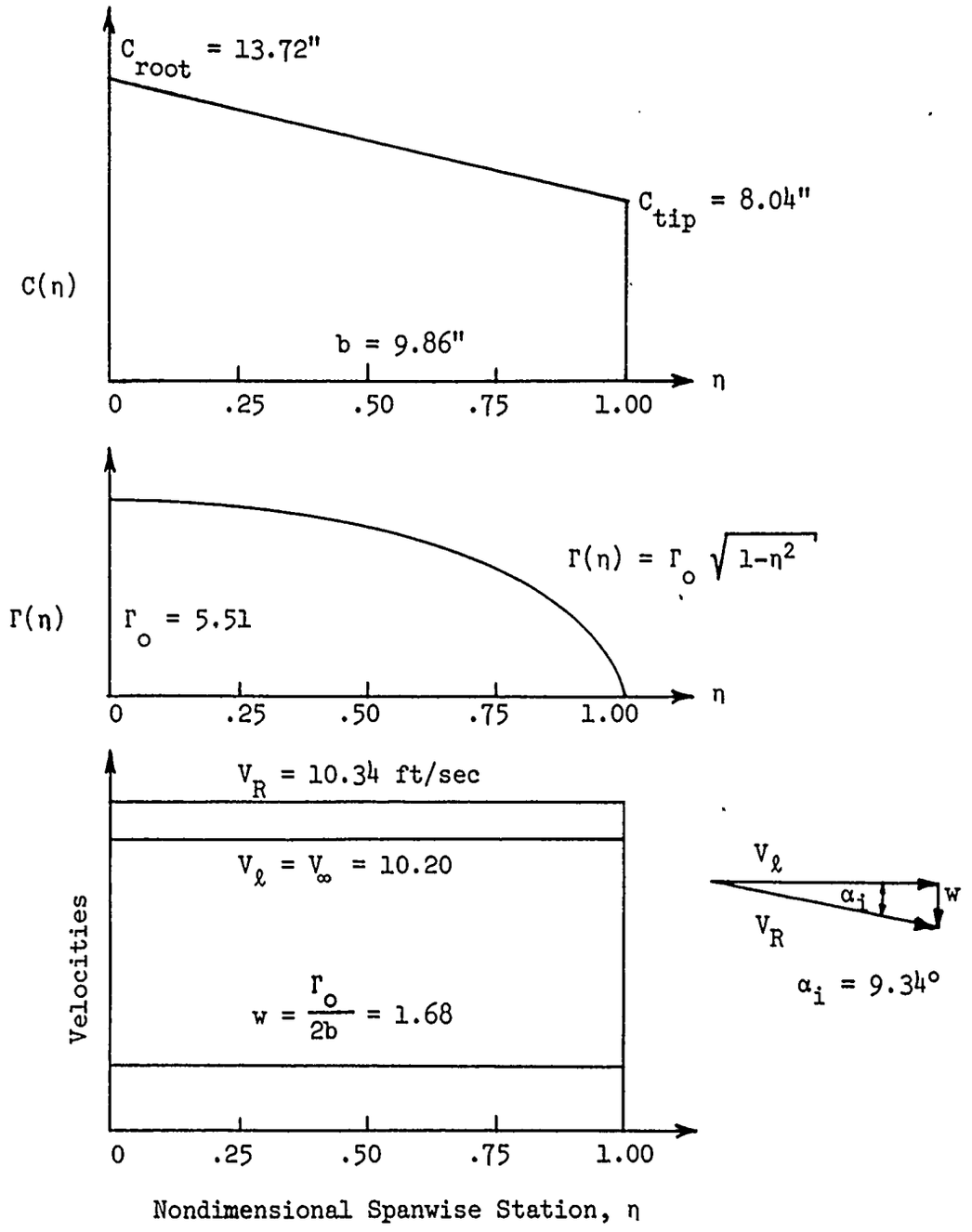

Figure 35 - Spanwise Distributions for Case II

(Simplified Circulation Assumption)

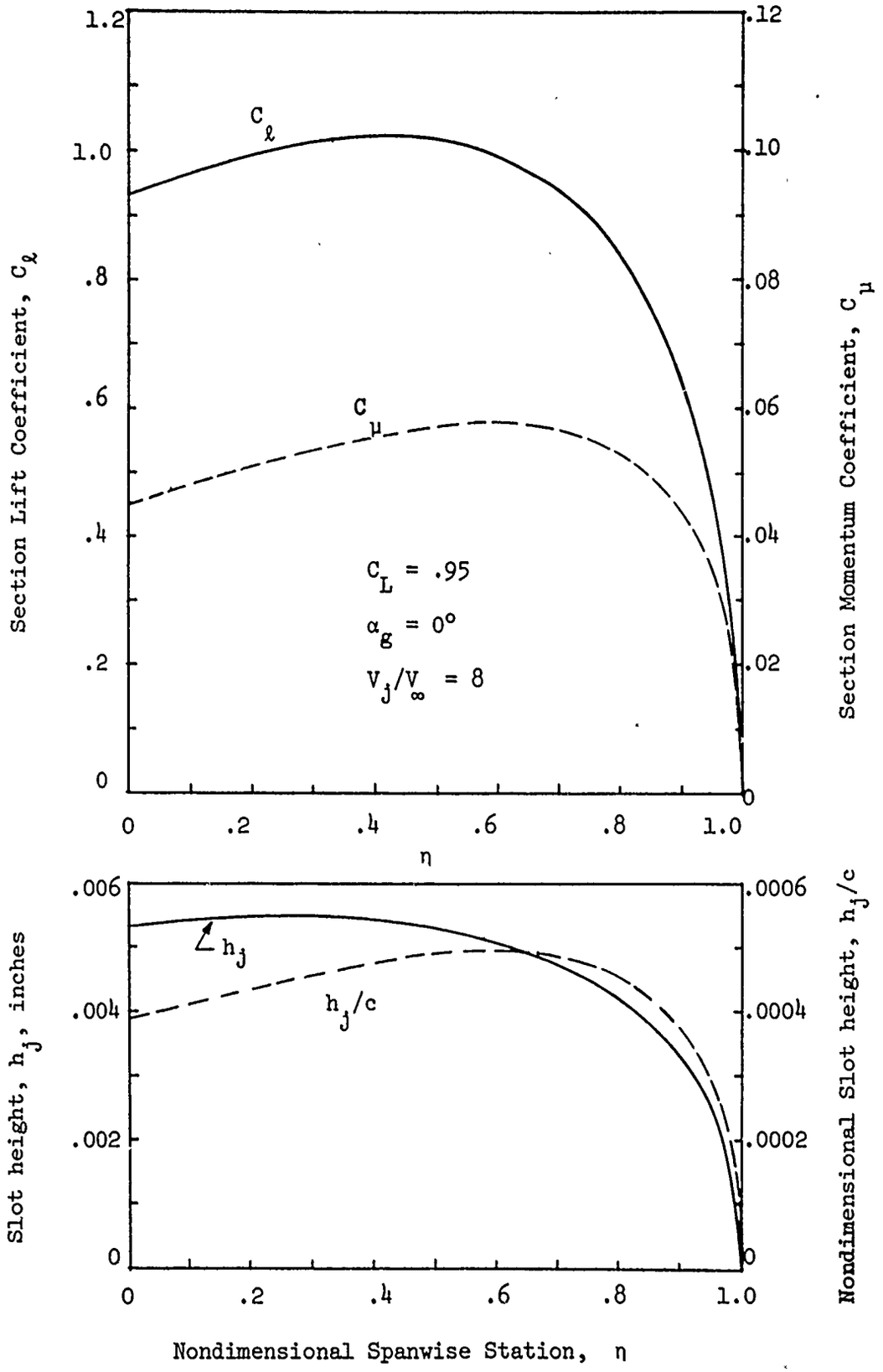

Figure 36 - Resulting Spanwise Distributions for Case II

UNCLASSIFIED
Security Classification

DOCUMENT CONTROL DATA - R & D

(Security classification of title, body of abstract and indexing annotation must be entered when the overall report is classified)

1 ORIGINATING ACTIVITY (Corporate author)	2a. REPORT SECURITY CLASSIFICATION
Aviation and Surface Effects Department Naval Ship Research and Development Center Bethesda, Maryland 20034	Unclassified 2b. GROUP

3 REPORT TITLE

DESIGN OF A CIRCULATION CONTROL STERN PLANE FOR SUBMARINE APPLICATION

4 DESCRIPTIVE NOTES (Type of report and inclusive dates)

Technical Note

5. AUTHOR(S) (First name, middle initial, last name)

Robert J. Englar and Robert M. Williams

6. REPORT DATE	7a. TOTAL NO. OF PAGES	7b. NO. OF REFS
March 1971	73	11

8a. CONTRACT OR GRANT NO.	9a. ORIGINATOR'S REPORT NUMBER(S)
b. PROJECT NO.	Technical Note AL-200
c. Task No. ZR 011 0101	9b. OTHER REPORT NO(S) (Any other numbers that may be assigned this report)
d. NSRDC No. 564-009	

10. DISTRIBUTION STATEMENT Distribution limited to U.S. Government agencies only; Test and Evaluation; March 1971. Other requests for this document must be referred to Head, Aviation and Surface Effects Department.

11. SUPPLEMENTARY NOTES	12. SPONSORING MILITARY ACTIVITY
	Commander Naval Material Support Activity (03L4) Washington, D.C. 20360

13. ABSTRACT

This

The present study was undertaken to design a non-deflecting circulation control (CC) submarine stern plane to provide maneuverability control and eliminate the possibility of catastrophic crash dives due to stern plane jamming. Symmetric elliptic sections with tangential blowing out of upper and lower slots over a rounded trailing edge were used because of their high lift and equivalent aerodynamic (hydrodynamic) efficiencies. The CC model stern plane so designed was restricted by the requirement to maintain the same planform as a conventional stern plane, by the existence of a large boundary layer on the main body, and by the additional requirement of zero deflection. With moderate blowing, it was able to meet or exceed the prescribed lifting (maneuvering) requirements for the conventional deflecting control surface. In the event of a blowing failure, inherent stability would result due to the fixed nature of the plane. Presented in the study contains a detailed design procedure, supporting experimental data, and the final geometry of the blown model stern plane. Also included is a similar study on an alternate blown configuration with end plates which showed a considerable performance improvement over the first design.

DD FORM 1 NOV 65 1473 (PAGE 1)

S/N 0101-807-6801

Unclassified
Security Classification

14 KEY WORDS	LINK A		LINK B		LINK C	
	ROLE	WT	ROLE	WT	ROLE	WT
non-deflecting stern plane						
circulation control						
tangential blowing						
maneuverability control						
inherent stability						
finite wing						
elliptic airfoils						
end plates						
parabolic boundary layer						
induced velocity						